Top Curr Chem (2003) 226: 119 – 172
DOI 10.1007/b 10827

# Mineral Liquid Crystals from Self-Assembly of Anisotropic Nanosystems

Jean-Christophe P. Gabriel[1], Patrick Davidson[2]

[1] Nanomix, Inc., 5980 Horton Street, Suite 600, Emeryville, CA 94608, USA
*E-mail: jcgabriel@nano.com*
[2] Laboratoire de Physique des Solides, Bât. 510, UMR 8502 CNRS, Université d'Orsay, 91405 Orsay, France, *E-mail: davidson@lps.u-psud.fr*

In this article we review the mesogenic properties of the mineral liquid crystals (MLCs) based on molecular nanowires: $Li_2Mo_6Se_6$; nanotubes: Imogolite and $NaNb_2PS_{10}$; molecular ribbons: $V_2O_5$; exfoliated single sheets: smectic clays and $H_3Sb_3P_2O_{14}$; nanorods: Boehmite ($\gamma$-AlOOH), Akaganeite ($\beta$-FeOOH ), Goethite ($\alpha$-FeOOH); platelets: Gibbsite ($Al(OH)_3$ ); disks: $Ni(OH)_2$; bio-mineral hybrids. We then propose numerous phases that could lead to the discovery of new MLCs. We finally review how the properties of these mesophases and their collective behavior have been used for making mesoporous composites with anisotropic properties, for making nanodevices and solar cells, as well as how they could be used to allow the measurement of residual dipolar couplings in NMR studies of biomolecules.

**Keywords.** Liquid crystals, Complex Fluids, Self-assembly, Mineral, Inorganic, Nanosystem, Nanoparticle, Nanotube, Nanowire, Nanorod, Anisotropy, NMR

## List of Abbreviations

| | |
|---|---|
| AAO | Anodic Aluminum oxide |
| AOT | (2-Ethylhexyl)sulfosuccinate |
| CNT | Carbon nanotube |
| CVD | Chemical vapor deposition |
| DLVO | Deryagin Landau Verwey Overbeek |
| DMF | Dimethylformamide |
| DMSO | Dimethylsulfoxide |
| FFEM | Freeze fracture electron microscopy |
| FWHM | Full width at half maximum |
| HFCVD | Hot filament chemical vapor deposition |
| HPC | Hydroxypropylcellulose |
| HT | High temperature |
| MLC | Mineral liquid crystals |
| NMF | *N*-Methylformamide |
| NR | Nanorod |
| NT | Nanotube |
| NW | Nanowire |
| PBLG | Poly($\gamma$-benzyl-L-glutamate) |
| PDMS | Poly(dimethylsiloxane) |
| PVA | Poly(vinylalcohol) |
| SANS | Small Angle Neutron Scattering |
| SAXS | Small angle X-ray scattering |
| TEM | Transmission electron microscopy |

TMV Tobacco Mosaic Virus
USAXS Ultra small angle X-ray scattering

## 1 Introduction

Liquid crystalline phases, which were discovered more than a century ago, are phases intermediate between crystalline and liquid ones [1]. They combine both the fluidity of the liquids and the anisotropy of crystals and they are usually based on anisotropic building blocks (molecules, polymers, micelles, aggregates etc...). Liquid crystalline materials are extremely diverse since they range from DNA to Kevlar (a high strength synthetic polymer) and from small organic molecules used in displays to self assembling amphiphilic soap molecules. A common feature of all these materials is that they are organic [2] or organometallic – ca. inorganic – and currently there are more than 80,000 examples of organic liquid crystalline compounds [3]. In contrast, there are only a dozen lyotropic mineral liquid crystals known and characterized to date [4]. One reason is that there are only a few low-dimensional (one-dimensional or two-dimensional) purely-inorganic objects known to dissolve or to be dispersed in water or in other organic solvents. The solubility criteria of mineral moieties, their interactions with solvents, and the structures and physical properties of such fluids are currently a subject of intense research activity [4, 5]. In addition, organic synthesis techniques allow numerous structural variations of liquid crystalline molecules to be made whereas the solution chemistry of molecular mineral objects, i.e., prepared by high temperatures solid state reactions, is still being developed [6].

Concerning the use of the term "mineral" to name this family of liquid crystals, one can argue that the term inorganic would be more appropriate. However, inorganic liquid crystals have long been used for organometallic liquid crystals [7]. Therefore in order to avoid any confusion between these fairly chemically different families, and taking into account that a large number of these liquid crystals occur naturally in nature, we think that the use of the old fashioned but adequate "mineral" adjective taken sensus largo is more specific that an alternative such as "purely inorganic", to name this subclass of the inorganic liquid crystals family.

In spite of their scarcity, lyotropic mineral liquid crystals have actually been known for many decades: Zocher, a German scientist, reported as early as 1925 the observation of the unusual behavior of colloidal aqueous suspensions of vanadium pentoxide ($V_2O_5$) [8]. He compared these suspensions with the newly discovered liquid crystalline phases and inferred that these colloids must be constituted from needle-like objects mutually oriented in the same direction. We know now that this behavior in fact arises from $V_2O_5$ ribbons forming a nematic phase. Later, in 1938, Langmuir examined suspensions of bentonite clay platelets and recognized their anisotropic and fluid-like properties [9]. However, the key theoretical development came with the theory that Onsager devised to describe the nematic ordering of suspensions of rod-like particles such as the Tobacco Mosaic Virus (TMV) [10]. This model provides an extremely useful frame to un-

derstand and predict this kind of phase transition in mineral and organic systems. This model which is based on simple assumptions describes in quantitative terms the phase diagram for any suspension of anisotropic rod-like (or disk-like) particles interacting solely through a hard-core potential and predicts that it should undergo a nematic/isotropic first-order transition (i.e., with phase coexistence) and that temperature has no effect on this transition. Numerical simulations have also proved to be very powerful techniques to gain insight into such phenomena [11].

From the experimental point of view, a simple way to identify a liquid crystalline phase is to observe its texture using polarized light microscopy. Unlike usual isotropic liquids, liquid crystalline phases are birefringent, interact with linearly polarized light, and can be observed between crossed polarizers. The detection of birefringence when the fluid phase is at rest proves that it is liquid crystalline. The textures observed under polarized light are due to the existence of topological defects and their analysis gives information on the symmetry of the phase. For instance, the most common defects of the nematic phase are called disclination lines. These are one-dimensional singularities in the local average direction (director) of the anisotropic moieties. Thus, unless special caution is taken to remove these defects, nematic samples are usually "powders" (i.e., random distributions) of small nematic domains (a "nematic domain" is defined as a region of the sample which shows ideal nematic orientational correlation).

Nematic phases can often be aligned by the action of a magnetic field. The alignment is due to the anisotropy of the mesophase that reorients to minimize its free energy in the field. Therefore, the director is aligned along or perpendicular to the field direction, depending on the sign of the magnetic anisotropy of the building blocks. The alignment of the phase in an external field suppresses the topological defects and produces a single domain that is suitable for more detailed physical studies. Electric fields produce similar effects: this is the basis of most applications of nematic phases in display technology.

Small angle X-ray scattering (SAXS) is a powerful technique [12] to study the molecular organization of lyotropic nematic phases on a length scale ranging from 3 to 300 nm. In this range, the detailed atomic structure of the particles is irrelevant and the scattering is sensitive to only the particle shape and its electronic contrast with the solvent. In this respect mineral liquid crystals are particularly convenient because their contrast is usually much larger than that of their organic counterparts. SAXS also allows a clear-cut demonstration of the symmetry and structure of a complex fluid, avoiding possible and usual pitfalls that can come when one restricts itself to only a texture analysis.

In contrast to organic liquid crystals, mineral liquid crystals can differ largely in size from one system to another. They actually range from molecular nanowires or nanotubes to anisotropic crystallites such as nanorods. Molecular nanowires can be considered as one-dimensional objects where the diameter is precisely defined by the molecular unit that makes up the chain (typically 5–25 Å). In contrast, molecular disks (nanosheets) are two-dimensional objects where the thickness of the disks is defined at the molecular scale but the diameter is polydisperse (100–10,000 Å). Finally, liquid crystalline suspensions may

be formed from anisotropic crystallites whose dimensions are all in the colloidal range (100–10,000 Å) so that these moieties are two to three orders of magnitude larger than usual organic liquid crystals. This classification defines the outline of this review article.

## 2 Molecular Nanowires

### 2.1 Dispersion of a Conducting Nanowire: $Li_2Mo_6Se_6$

Among all the phases that have been discovered after the report of high critical field superconductivity within the Chevrel-Sergent phases ($MMo_6X_8$–M=Cu, Pb, Sn, etc.; X=S, Se, Te), $Li_2Mo_6Se_6$ is singular since it contains $^1_\infty[Mo_6Se_6]^{2-}$ infinite conducting molecular nanowires [13, 14] and, it has been demonstrated to be soluble in highly polar solvents such as *N*-methylformamide (NMF) or dimethylsulfoxide (DMSO) [15][1]. It is this last property that prompted us to investigate such solutions and therefore led us to study mineral liquid crystals. The infinite mineral polymer $^1_\infty[Mo_6Se_6]^{2-}$ (Fig. 1d) can be regarded as a stack of dimerized $Mo_3Se_3^-$ units (Fig. 1a), and therefore is the end member (n=∞) of the $(Mo_3Y_3^-)_nY_2$ series (Y=chalcogen) (Fig. 1b, c). The study of static solutions of $Li_2Mo_6Se_6$ in NMF ($c>10^{-2}$ mol $l^{-1}$) with an optical microscope under polarized light (crossed polarizers) has demonstrated their birefringent and thus anisotropic nature. Both threaded and Schlieren textures were revealed [16], which are textures usually observed in the case of organic nematic phases and prove the mesogenic nature of these solutions.

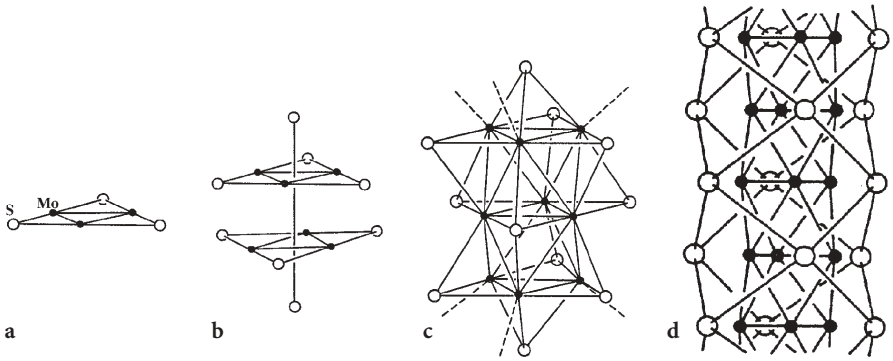


**Fig. 1a–d.** $Li_2Mo_6Se_6$ can be seen as the end member of the family $(Mo_3Se_3^-)_nSe_2$ made from the alternating stacking of $Mo_3Se_3^-$ motifs with an extra chalcogen capping each extremity: **a** n=1; **b** n=2; **c** n=4; **d** n=∞

[1] Note that $^1_\infty[Mo_6Se_6]^{2-}$ solutions are not stable for more than a few hours when in contact with dioxygen because of the decomposition of the chains. However, they can be kept for months and even years if kept or sealed under an inert atmosphere.

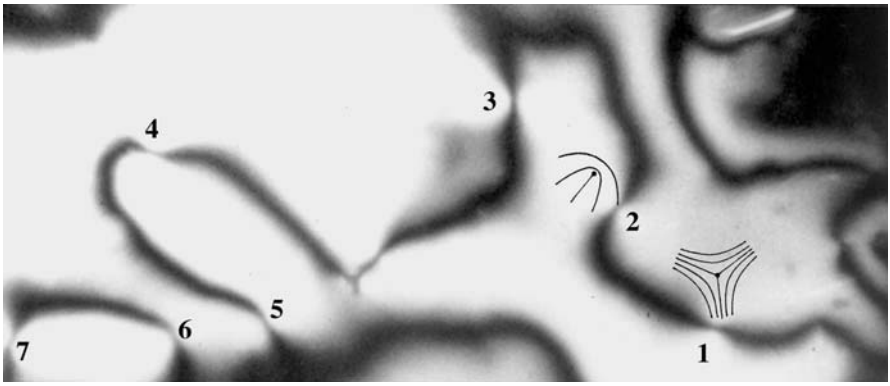


**Fig. 2.** Photograph of a typical Schlieren texture obtained from a $10^{-1}$ mol $l^{-1}$ solution of $Li_2Mo_6Se_6$ in *N*-methylformamide in the nematic phase taken using an optical microscopy with crossed polarizers with a magnification of 1000x. (Reprinted from [4b], copyright (2000) from John Wiley and Sons)

For example, Fig. 2 shows a Schlieren texture, which is typical of nematic distortions of the director field (visible as dark branches usually named *brushes*). These distortions are induced by the perpendicular anchoring on the microscope slide of topological defects, called disclination lines, which are numbered from 1 to 7 in Fig. 2. These disclination lines can be classified into two groups according to their local topology as the dark brushes seen around these defects can rotate either clockwise or counterclockwise as the crossed polarizers are rotated simultaneously while the sample is kept fixed. This is due to the two different possible defect topologies illustrated in Fig. 2 for cases 1 and 2 [1].

The structure of these fluids was investigated by X-ray diffraction. When the chains are fully exfoliated the full width at half maximum (FWHM) of the (002) peak characteristic of the distance separating two $Mo_3Se_3^-$ moieties along the chain is of the same order as the experimental resolution; hence the coherence length of the chains is at least 1000 Å [17].

The anisotropic X-ray scattering pattern shows that there is no long-range three-dimensional positional order, demonstrating that this fluid is of a nematic liquid-crystalline nature (Fig. 3a). Moreover, the observation of an interference peak in Fig. 3b proves the existence of short-range positional correlations at ~70 Å, due to the separation of the chains, and probably arising from their repulsive electrostatic interactions. Indeed, charged particles confined in a finite volume at thermodynamic equilibrium repel each other and therefore stay at a well defined distance. Note that the diffuse ring of Fig. 3b appears anisotropic, indicating partial orientation of the chains along the capillary axis.

In addition to nematic ordering observed for the system $Li_2Mo_6Se_6$/solvent, the monodispersity in diameter of the wires should allow one to observe a nematic-hexagonal transition at high concentration. Note that, when the proper solvent is used (in order to avoid formation of bundles), one can expect to be able to tune the distance between the wires just by changing the concentration.

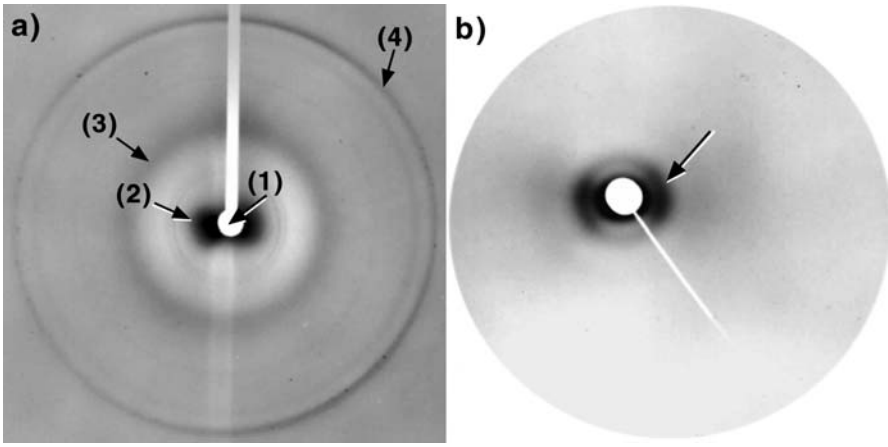


**Fig. 3a,b.** X-ray diffraction patterns obtained from a capillary filled with $10^{-1}$ mol $l^{-1}$ solution of $Li_2Mo_6Se_6$/NMF: **a** using wide angle scattering. (**1** is the beam stop shadow, **2** the small angle scattering, **3** the diffuse scattering ring due to the solvent, **4** the 002 diffraction peak); **b** small angle scattering showing the presence of a diffuse ring at $q=9\cdot10^{-2}=2\pi/70$ $Å^{-1}$ (*arrow*)

This is indeed a typical behavior for dispersion of 1-D nanostructures (2-D swelling).

More recently, the molecular nanowire $Mo_6Se_6^{2-}$ has become a fairly popular subject of investigation due to the rise of nanotechnology [18] and the scarcity of well-defined molecular wires available that can be dispersed in solution. In one such study, $Mo_6Se_6^{2-}$ nanowires were dispersed and recondensed using a surfactant. Dense phases were obtained with lamellar or hexagonal ordering of the wires, depending upon the surfactant used. Furthermore, the distance between the $Mo_6Se_6^{2-}$ wires in these condensates could be adjusted by varying the number of carbon atoms in the aliphatic chain of the surfactant [19]. In a similar dispersion-recondensation study, P. Yang and co-workers used the self-assembly properties of $Li_2Mo_6Se_6$-solvent to perform a cation exchange of the Li with more bulky cations such as $Na^+$, $K^+$, $Rb^+$, $Cs^+$, $NMe_4^+$. This was performed by retaining the lithium cation in solution using 12-crown-4 ether [20].

Other studies focused on the electrical properties of discrete nanowires in a similar way that has been done with nanotubes. However the lack of stability of this phase when in contact with oxygen makes these studies experimentally difficult [21].

The example of $Li_2Mo_6Se_6$ illustrates one synthetic method towards low dimensional mineral compounds, commonly referred to as the "shake and bake" method. It usually implies the mixing of the starting materials followed by a high temperature treatment. Then, in order to obtain a liquid crystal, one needs to bring these charged low-dimensional mineral anions into solution. Thus, how can one control, within a given ternary or quaternary system, the dimensionality of the synthesized polymeric compounds? This problem has been addressed in the literature and an answer, based upon the 8-N electron rule, can be found

when using alkali metals (or other strong electropositive metals) as cations [22, 23]. Transferring electrons from the alkali metal to a 3-D polymeric covalent framework usually results in some of the covalent bonds being replaced by negative charges, hence the dimensionality of the framework is reduced, producing covalent negatively charged fragments, separated by alkali cations. By increasing the alkali metal content, further dismantling of the framework structure can be induced to the point where the residual framework is of molecular dimensions. This method is most efficient when large alkali metals such as cesium are used, because increasing the separation between the low dimension anionic moieties minimizes their electrostatic repulsion. A consequence of this is that a synthesis successful with cesium may not necessarily work with lithium (for example, the synthesis of $Li_2Mo_6Se_6$ differs from the one of $In_2Mo_6Se_6$ in the fact that it cannot be achieved directly at high temperature from the native element but required a two step synthesis, including an ion exchange procedure). This can be a problem in order to get soluble phases since it is empirically observed that in an alkali series of a given anion the highest solubility is obtained with the smallest cation [24]. Thus, a delicate balance needs to be found in order to synthesize new soluble low dimensional phases and, when the targeted phase cannot be directly synthesized with the smallest cation, a cation exchange additional step should be applied. This can either be tried in the solid state by a clever use of the different sublimation temperature to induce the cation exchange, or indirectly in solution by using high concentration of the replacing cation. In the latter case, it should be noted that the smallest cation that can be used is in fact $H^+$, for phases that can handle acidic conditions.

## 2.2
## Imogolite: A Natural Nanotube, Aqueous Synthesis, and Composite Materials

Imogolite is a natural hydrated aluminum silicate first discovered in 1962 in the clay fraction of Japanese volcanic ash and it is found widely distributed in recent volcanic deposits. Since 1977, it is possible to synthesize it in the laboratory from dilute aqueous solutions of hydroxyaluminum cations and orthosilicic acid [25] or, by reaction of tetraethylorthosilicate with an aluminum source (aluminum chloride or aluminum *sec*-butoxide) [26, 27], at temperatures ranging from 25 to 100 °C.

This compound is made up of hollow rigid molecular tubes of diameter 25 Å and of variable length (Fig. 4). These can be dispersed in acidified water solutions [28]. A Japanese group has demonstrated that, in a specific range of concentrations, these suspensions phase separate into an isotropic liquid phase and a birefringent one [29]. Temperature has no influence on this phase transition. Fingerprint textures have been observed under polarized light, which, though highly reminiscent of cholesteric (i.e., chiral nematic) textures, have finally been attributed to the existence of a pleated structure on the basis of electron microscopy investigations of freeze-dried samples [30]. These studies show that the pleated sheets consist of a nematic organization of imogolite tubes. This prompts a comparison with the precholesteric states of DNA or collagen [31]. The phase transition could be explained on the basis of the Onsager

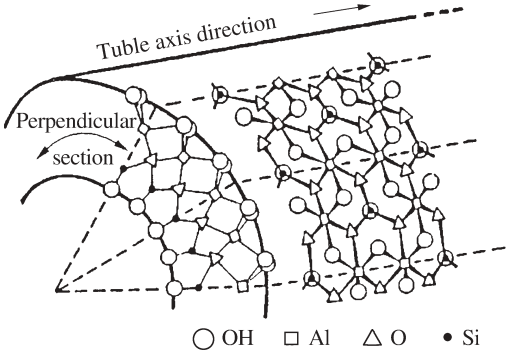


**Fig. 4.** Schematic view of part of an imogolite cylinder formed from twelve gibbsite structural type units, each corresponding to $(Al_2O_3 \cdot SiO_2 \cdot 2H_2O_2)_2$) and indicated by *dotted lines* (Reprinted from [29a], copyright (1986) from John Wiley and Sons)

model and the specific effects of polydispersity of the tube length were studied in detail.

The same group has also obtained composite materials based on imogolite and water-soluble polymers such as hydroxypropylcellulose (HPC) and poly (vinylalcohol) (PVA) [32]. HPC is a rigid rod polymer that has a cholesteric phase, whereas PVA is a random coil amorphous polymer. Significantly enhanced mechanical properties were only obtained in the case of the HPC composite materials.

## 2.3
## Solvent Dependent Coiling of a Chain into a Nanotube: $NaNb_2PS_{10}$

In a recent search for other soluble mineral polymers, we discovered that $KNb_2PS_{10}$ was soluble in hot DMSO. Our attention was drawn to this structure because we suspected the $^1_\infty[Nb_2PS_{10}]^-$ chain to be of intermediate rigidity between the rigid $Mo_6Se_6^{2-}$ molecular nanowire and the highly flexible $KPdPS_4$. The latter was shown to be highly flexible and behaving very similarly to organic flexible polymers [6]. In order to increase the solubility of $KNb_2PS_{10}$ we synthesized its sodium equivalent $NaNb_2PS_{10}$ which, as expected, proved to be much more soluble in polar solvents. When observed under polarized light between crossed polarizers, concentrated solutions in NMF show strong flow birefringence. Such flow birefringence can arise either from a preferred orientation of anisotropic rigid molecules induced by the flow (like logs aligned with the flow in a river), or from stretching of entangled, folded, semi-flexible polymers (like drawn spaghetti).

SAXS investigation of the structure of these fluids showed a complex structure with two distinct features. The first signal demonstrated that upon dilution a 2-D swelling occurred, typical of suspensions of one-dimensional moieties. The second signal however was independent of the dilution and could not be explained by the chain structure; it is therefore the signature of a superstructure.

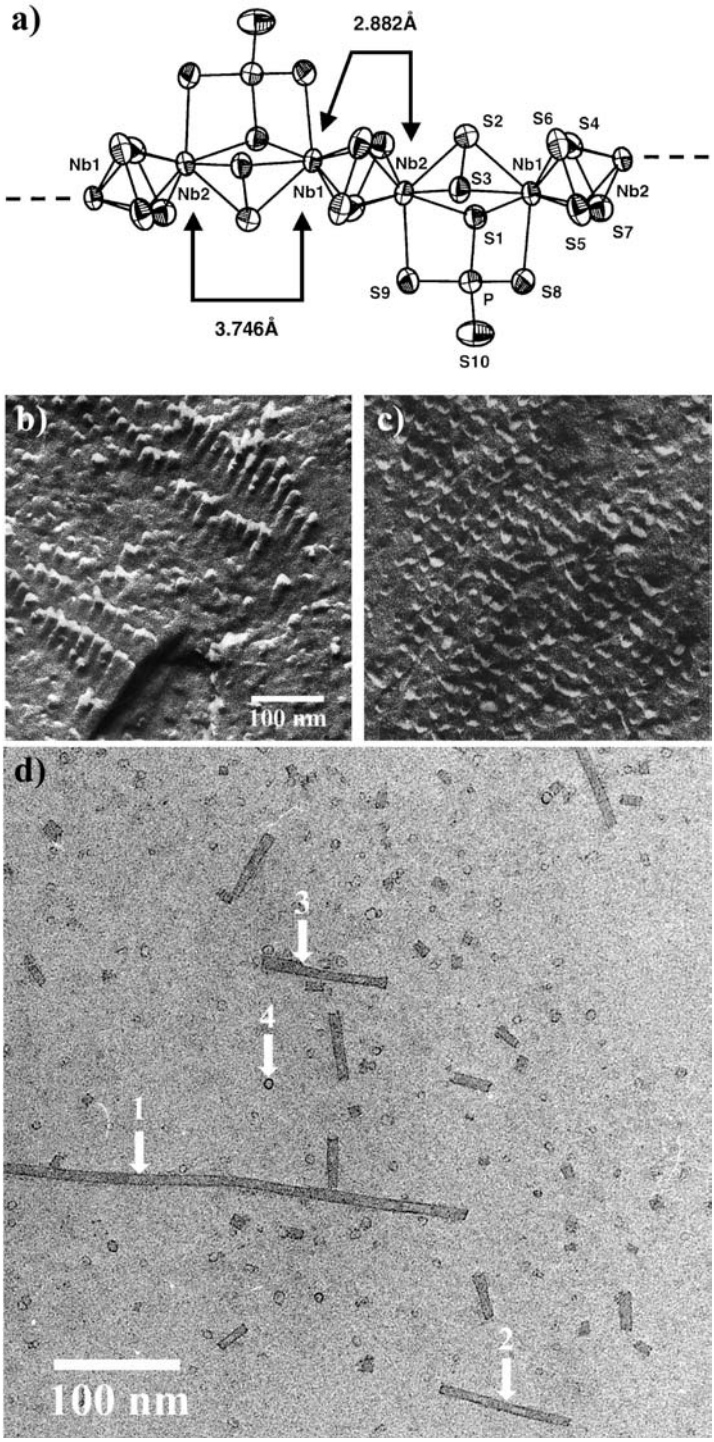
a)
2.882Å
Nb1
Nb2
Nb1
Nb2
S2
S6
S4
Nb1
Nb2
S3
S1
S5
S7
S9
P
S8
S10
3.746Å
b)
100 nm
c)
d)
3
4
1
2
100 nm

Furthermore, at higher concentration, thin diffraction lines were superimposed on the previously described signals, indicating that a first order transition toward a columnar mesophase (H) of hexagonal symmetry occurred. Partial alignment and even the melting (above 240 $s^{-1}$) of this hexagonal MLC could be obtained using a Couette shear cell. Such a melting had only been reported once prior to this study in the case of a hexagonal mesophase of a surfactant [33].

These results put together provide strong support for the presence in solution of cylinders having a well-defined diameter. However, a difference of behavior depending upon the solvent used was observed. If now DMF was used as the solvent, only the signature of 0-D moieties was detected. In addition no transition towards a hexagonal phase could be found.

To understand further and confirm our interpretation of the SAXS data, we complemented these results with a study using freeze fracture electron microscopy (FFEM) as well as low dose TEM (Fig. 5). This allowed us to show that in NMF $NaNb_2PS_{10}$ folds into single walled nanotubules having wall thickness of 1.6 nm (Fig. 5), whereas only globular coils can be observed in DMF. Furthermore, at high concentration in NMF these nanotubules tend to aggregate into bundles packed in a well-defined hexagonal arrangement [34].

A question still remains about the structure of the polymer within the walls of these nanotubules. The very low stability of theses tubes under TEM irradiation, even when applying low doses, precluded us so far from observing high-resolution images. An electron diffraction pattern highly reminiscent of a helicoidal organization of the polymer was observed but this still needs to be confirmed and studied in more detail.

## 3
## Molecular Ribbons: $V_2O_5$, a MLC that Can be Readily Aligned in Both Magnetic and Electric Fields

Another way of obtaining suspensions of anisotropic mineral moieties is by the spontaneous condensation of dissolved molecular species. A typical example of this process is the synthesis of $V_2O_5$ ribbons by using "chimie douce" (soft chemistry) techniques (Fig. 6) [35, 36]. At pH≈2, V(V) species exist in an octahedral coordination with a V=O bond pointing along the Oz axis, three V-OH bonds in the xOy plane, and two bonded $H_2O$ molecules to fill the coordination sphere. Beyond a concentration threshold of $10^{-3}$ mol $l^{-1}$, these vanadate species spontaneously condense in the xOy plane by two different reactions respectively called olation and oxolation reactions (olation: $V\text{-}OH+V\text{-}OH_2 \rightarrow V\text{-}OH\text{-}V+H_2O$; oxolation: $V\text{-}OH+V\text{-}OH \rightarrow V\text{-}O\text{-}V+H_2O$) to form ribbons 1 nm thick, about 25 nm

**Fig. 5.** **a** View of the $^1_\infty[Nb_2PS_{10}]^-$ chain showing the atom labeling and selected Nb-Nb bond lengths. **b,c** Arrays of nanotubules as observed by FFEM ($NaNb_2PS_{10}$ in NMF, 0.140 mol $l^{-1}$) with the cryofracture plane being arbitrary or perpendicular to the nanotubule axes for b and c, respectively. **d** Image obtained by low dose TEM of very dilute solutions of $NaNb_2PS_{10}$ in NMF showing single-wall nanotubules with: 10 nm ∅ (1), 7 nm ∅ (2), a 7–10 nm ∅ defect (3), and small rings corresponding to tubes seen along their principal axis (4). (Adapted from [34], copyright (2002) from the American Chemical Society)

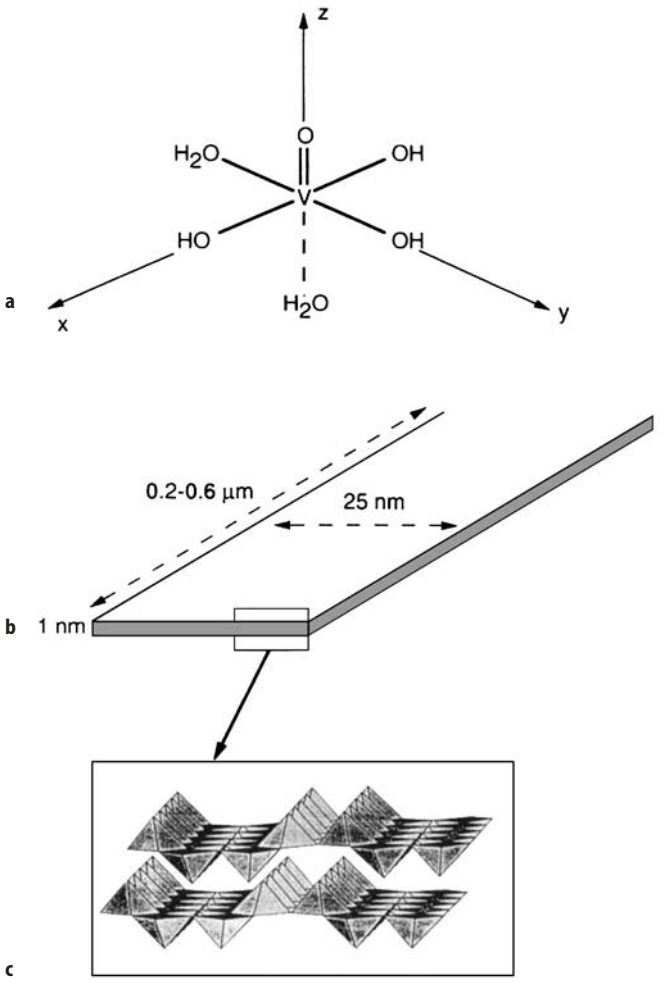


**Fig. 6.** **a** The molecular species that condense through olation and oxolation reactions into $V_2O_5$ ribbons **b** whose molecular structure is shown in **c**. (Reprinted from [4b], copyright (2000) from John Wiley and Sons)

wide, and about 200–600 nm long. The thickness is precisely defined by the ribbon molecular structure whereas both width and length is subject to some polydispersity, which is, however, usually rather small. The structure of these oxide ribbons is close to that of orthorhombic $V_2O_5$. The condensation reaction can be performed in several ways leading to similar ribbon structures. One of the most popular methods, as it avoids the introduction of foreign ions, consists of the acidification of an aqueous $NaVO_3$ solution by passing it through an ion-exchange resin column. The synthesis of $V_2O_5$ ribbons is a complex non-equilibrium process in which electrical charges play an important role. During the ola-

tion and oxolation reactions, V(V) charged molecular species are consumed and uncharged condensed moieties are produced. These condensed moieties do not experience electrostatic repulsion and hence flocculation of the suspension occurs under the influence of attractive Van der Waals interactions. However, this flocculation is only transient because subsequent adsorption and dissociation of water molecules produce V-OH groups, the ionization of which creates negative electrical charges on the surface of the ribbons and therefore repulsive electrostatic interactions become important again and ensure the stability of the colloid. Dark red gels and sols comprised of entangled ribbons dispersed in water are thus obtained.

The colloidal suspensions produced in this way are stable for years and, a few days after synthesis, their properties do not vary with time any more. In particular, they form a nematic liquid crystalline phase at volume fractions $\Phi$ larger than 0.7% [37]. Moreover, these suspensions undergo a sol/gel transition at $\Phi$=1.2% which divides the nematic domain into a nematic sol and a nematic gel. The optical textures of samples sealed in flat glass capillaries and observed under polarized light microscopy are indeed typical of a nematic phase. The nematic sol phase readily displays Schlieren textures whereas the nematic gel often shows the so-called "banded texture" of sheared nematic polymers caused by filling the flat glass capillaries with gel samples. Moreover, at volume fractions larger than 5%, SAXS experiments with samples aligned by shear, proved that $V_2O_5$ suspensions are in a biaxial nematic gel state [38].

An outstanding feature of the $V_2O_5$ nematic sols is that they can be aligned in quite moderate magnetic fields [39]. For example, for samples 0.1 mm thick, at a volume fraction of $\Phi \approx 0.8\%$, a magnetic field larger than 0.3 Tesla will align the $V_2O_5$ ribbons parallel to the field. The defects observed by microscopy then vanish and the texture becomes completely homogeneous, as expected for a nematic single domain. This means that mineral non-ferromagnetic objects can thus be aligned by a purely external non-invasive action. Once the magnetic field has been removed, the samples still keep their nematic single domain properties, which makes them suitable for other physical studies. The alignment of a $\Phi$=0.7% sample takes about 2 h at 0.3 T and about 5 min at 1 T. These times increase rapidly when $\Phi$ gets closer to the gelation threshold. Thus, $V_2O_5$ sols align as fast or even faster than usual lyotropic rigid rod polymers such as poly(*p*-benzamide) and poly($\gamma$-benzyl-L-glutamate) (PBLG) which respectively take hours or fractions of hours to align under similar conditions [40]. The magnetization of the phase is very small however and has not even been determined by a Squid magnetometer or by torque measurements. This means that the magnetization of the phase is actually comparable to that of pure water, a result which is understandable if one remembers the very small $V_2O_5$ volume fraction ($\Phi$=0.7%) involved. Consequently, the microscopic origin of the magnetic susceptibility and its anisotropy is still unknown. It has been proposed that the magnetization could arise either from a diamagnetism possibly related to the anisotropic shape of the ribbons or from the paramagnetism of V(IV) impurities always present at the level of a few percent. Nevertheless, this phenomenon illustrates a characteristic feature of "soft matter", namely that a very small perturbation can have a huge effect on the mesophase due to its collective nature. In other words, the

mineral building blocks of a nematic phase need not have strong magnetic properties for the phase to align in a magnetic field. In contrast, it was very difficult to induce any appreciable alignment in the isotropic phase of $V_2O_5$ ribbons.

An interesting application of the magnetic alignment is the following (Fig. 7). A single domain of the nematic phase can first be obtained by application of a magnetic field. Then, if this single domain is suddenly rotated in the field, it will undergo a transient hydrodynamic instability. This instability appears as a periodic pattern of microdomains in which the average direction of the ribbons is modulated. The pattern looks different depending upon the final magnetic field direction. This instability is classical in the field of liquid crystals and was thoroughly analyzed by Srajer et al. [41]. It can be used to micropattern a mineral material with periods in the range 10–100 μm in a very simple and cheap way. The lifetime of this instability varies from minutes to hours depending on the magnetic field intensity.

The production of nematic single domains also allows more detailed structural studies to be performed. For instance, the SAXS pattern (Fig. 8) of an aligned sample of $V_2O_5$ sol shows two diffuse spots located along a direction perpendicular to the director. These spots arise from the lateral interference between ribbons and their positions give the typical distance (~50 nm) between ribbons in the plane perpendicular to the director. This pattern is very similar to those of the nematic suspensions of the Tobacco Mosaic Virus (TMV), a typical example of rod-like organic polymer. Using a well-documented procedure, one can derive the nematic order parameter S from the distribution of scattered intensity [42]. This parameter takes values between 0, for a completely isotropic phase, and 1 for perfectly aligned moieties. The value obtained for $V_2O_5$, S=0.75, is in very good agreement with the predictions from the Onsager model and also, as expected, the nematic/isotropic phase transition is first order (with phase coexistence) and temperature has no influence on the nematic ordering (see also Sect. 5.1.). However, an increase of ionic strength, through salt (NaCl) addition had unexpected consequences. The nematic phase was actually stabilized with respect to the isotropic phase, in contrast to the behavior usually observed with this kind of lyotropic liquid crystals. This was attributed to Van der Waals interactions among ribbons that become increasingly important as electrostatic interactions are screened [43].

The anisotropy of the nematic phase also affects the properties of the solvent, in this case water. A recent $^2H$ NMR study of single domains of $V_2O_5$ sols has

**Fig. 7a–d.** Texture photographs in polarized light of transient hydrodynamic instabilities induced by a sudden change of the magnetic field orientation: **a** starting from a powder sample; **b** the magnetic field is applied along the main capillary axis; **c** the magnetic field direction is now perpendicular to the main capillary axis, but still in the plane of the figure. In consecutive stripes, the ribbons point in two different but symmetrical directions with respect to the polarizer-analyzer directions, giving rise to a zigzag pattern; **d** the magnetic field direction is now perpendicular to the plane of the figure. The dark regions are areas where the ribbons are perpendicular to the plane of the figure whereas the bright regions are areas where the ribbons still lie in the plane of the figure. (Reprinted from [39], copyright (1997) from John Wiley and Sons)

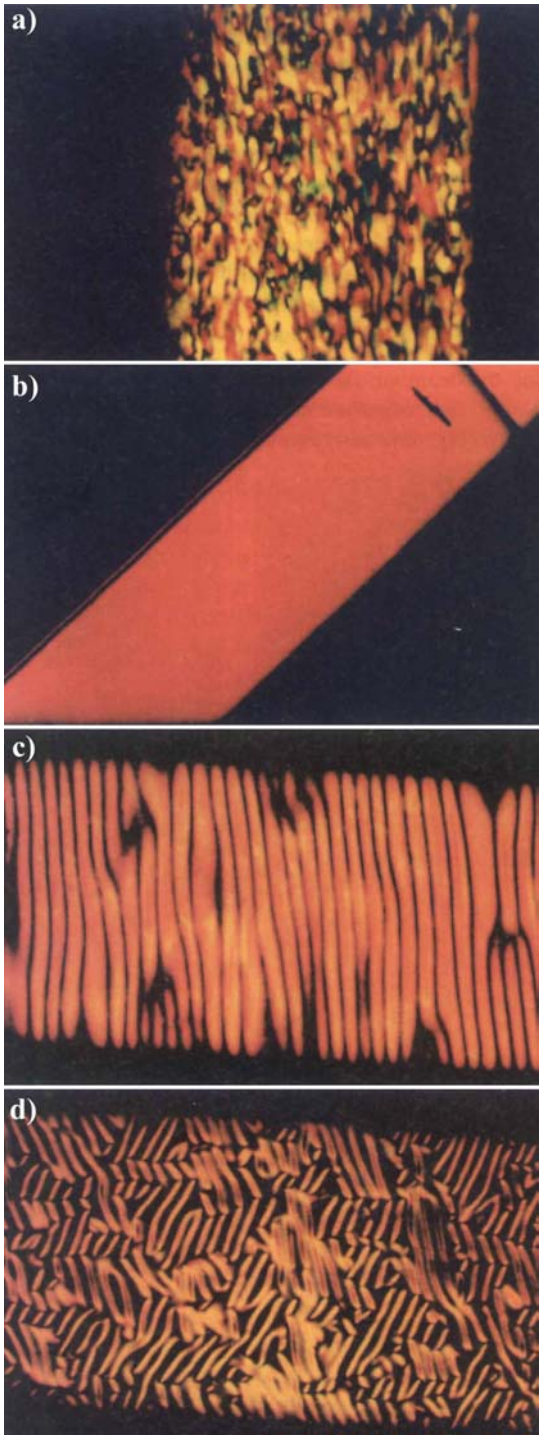
a)
b)
c)
d)

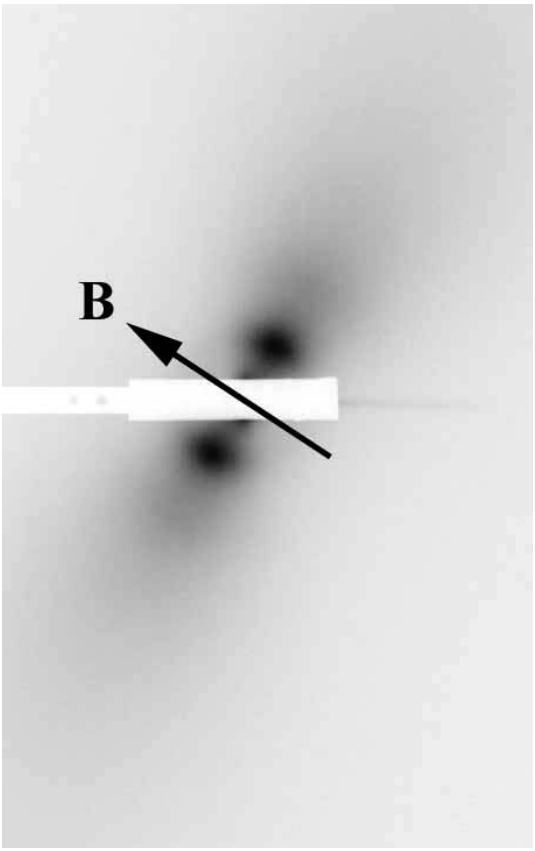


**Fig. 8.** Small angle X-ray scattering pattern of a sample aligned in a 1 T magnetic field. B is the field direction, which is set at an arbitrary angle of ≈40° to the main capillary axis. The *white rectangle* at the center of the figure is due to the beam stop

shown that, even at volume fractions as low as 0.7%, water molecules still experience a residual anisotropic interaction due to a situation of fast exchange between the bulk and sites located on the surface of the ribbons [44]. This is surprising and indicates that water molecules adsorbed on the surface of the ribbons still undergo fast motions. Thus, the behavior of the solvent faithfully reflects the anisotropy of the nematic phase, a feature that has subsequently been used to study the reorientation dynamics of the mesophase.

The magnetic alignment of these materials may be useful for applications when highly oriented samples are needed. $V_2O_5$ gels are classical host materials for the intercalation of guest species. For instance, the oxidative intercalation-polymerization of organic molecules, such as aniline or thiophene, has led to the synthesis of hybrid organic-inorganic materials, in which organic electrically conducting polymers are inserted between $V_2O_5$ ribbons giving rise to novel

sandwich compounds. This process, carried out in a magnetic field, may yield highly oriented conducting polymers of better quality.

Since one of the most important applications of liquid crystals lies in the electro-optic display industry, it was natural to examine the influence of an electric field on the nematic phase of $V_2O_5$ suspensions [45]. A major problem, due to the lyotropic nature of this liquid crystal, is the screening of the field by mobile ions. This was overcome by the use of a high frequency (300 kHz) a.c. field and of blocking electrodes. Home-made cells (thickness 10–75 μm) were prepared with glass plates coated with indium tin oxide electrodes covered with $SiO_2$ and polyimide layers. The cells were filled by capillarity. Applying fields of about 1 V $\mu m^{-1}$ was enough to align the phase from an initially planar texture to a homeotropic one. This reorientation is reversible so that switching cycles could be produced, using effective voltages of about 10 V. The response times are in the region of 1 s. In addition, the isotropic phase shows a very strong birefringence induced by the electric field. These properties formally demonstrate that mineral liquid crystals would have the potential for simple slow display applications.

## 4
## Molecular Disks

### 4.1
### Clays, Nematic Ordering vs Gelation

Clays of the montmorillonite family are lamellar aluminosilicates [46] used in many industrial processes and in products such as paints, softeners, and composite materials [47]. They swell when brought into contact with water, which is due to the insertion of water molecules between the sheets. Complete exfoliation can be induced leading to dispersions of disk-like particles of 10 Å thickness and 300–3000 Å in diameter, depending on the variety of clay used. These clay platelets bear a rather large surface electrical charge so that electrostatic interactions between them must be considered and are actually responsible for the colloidal stability of these dispersions. These suspensions have been widely studied as model colloids and also because they form physical thixotropic gels.

As early as 1938, Langmuir observed the phase separation of clay suspensions into an isotropic phase and a birefringent gel at the macroscopic level in test-tubes [9]. However, in the same report, he noted that this property of phase separation was gradually lost with time, which he tentatively explained by the incorporation of impurities diffusing from the glass tubes. He also compared this system to normal liquid crystals. Later, in 1956, Emerson observed a banded texture similar to that displayed by the Tobacco Mosaic Virus [48]. The investigation of clay suspensions from the structural point of view has been recently resumed. However, the study of the nematic order of suspensions of montmorillonite clays is in fact complicated by their gel properties. In spite of sustained efforts to understand its nature, the gelation mechanism has not yet been fully elucidated [49].

The role of the surface electrical charge is certainly crucial because the properties of the suspensions vary considerably with their ionic strength.

Quite recently two systems of the montmorillonite family, namely bentonite $[Na_x(Al_{2-x}Mg_x)(Si_4O_{10})(OH)_2,zH_2O]$ and laponite B $[(Na_2Ca)_{x/2}(Li_xMg_{3-x})(Si_4O_{10})(OH)_2, z\ H_2O]$ (an industrial form of hectorite) have been studied under polarized light using both the naked eye and optical microscopy [50]. The microscopic textures of concentrated gels (Fig. 9) are typical nematic ones. However, the nematic-isotropic phase separation has only been achieved very exceptionally, which seems to be a typical feature of these systems. In contrast with $V_2O_5$ ribbons, as the clay concentration increases, the suspensions, initially isotropic-liquid, become isotropic-gel and finally birefringent-gel (Fig. 10a,b). Temperature seems to have no influence on the nematic organization; the system is athermal as expected from the Onsager description that also applies to discs [51]. The isotropic gels show very large pretransitional effects such as flow and shock birefringence (Fig. 10c). The question about the thermodynamic nature of the birefringence of these gels naturally arises. In other words, is this birefringence due only to the freezing of some accidental flow birefringence or is it really intrinsic? Some simple experiments point to the thermodynamic nature of the nematic ordering. First, for one system, Langmuir has reported the phase separation of these suspensions. Second, the optical textures of these birefringent gels still slowly evolve over a few weeks after their preparation because topological defects anneal. However, the birefringence of these gels does not de-

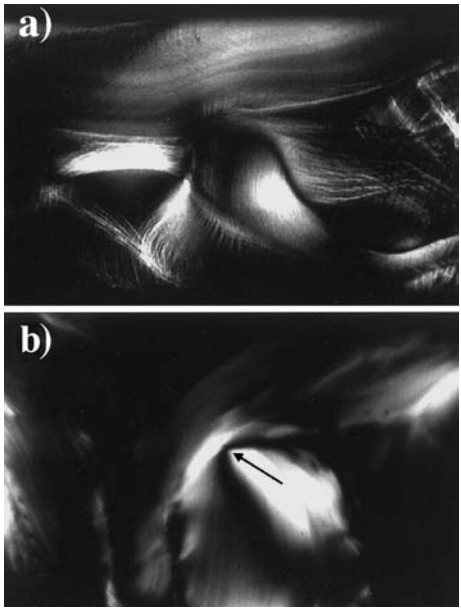


**Fig. 9a,b.** Microscopic observations in polarized light of the textures of the aqueous clay suspensions: **a** nematic threaded texture of a bentonite suspension (concentration 0.044 g/cm$^3$, magnification 50×); **b** detail of a 1/2 disclination line (*arrow*) in a laponite suspension (concentration 0.034 g/cm$^3$, magnification 100×) (Reprinted from [50], copyright (1996) from the American Chemical Society)

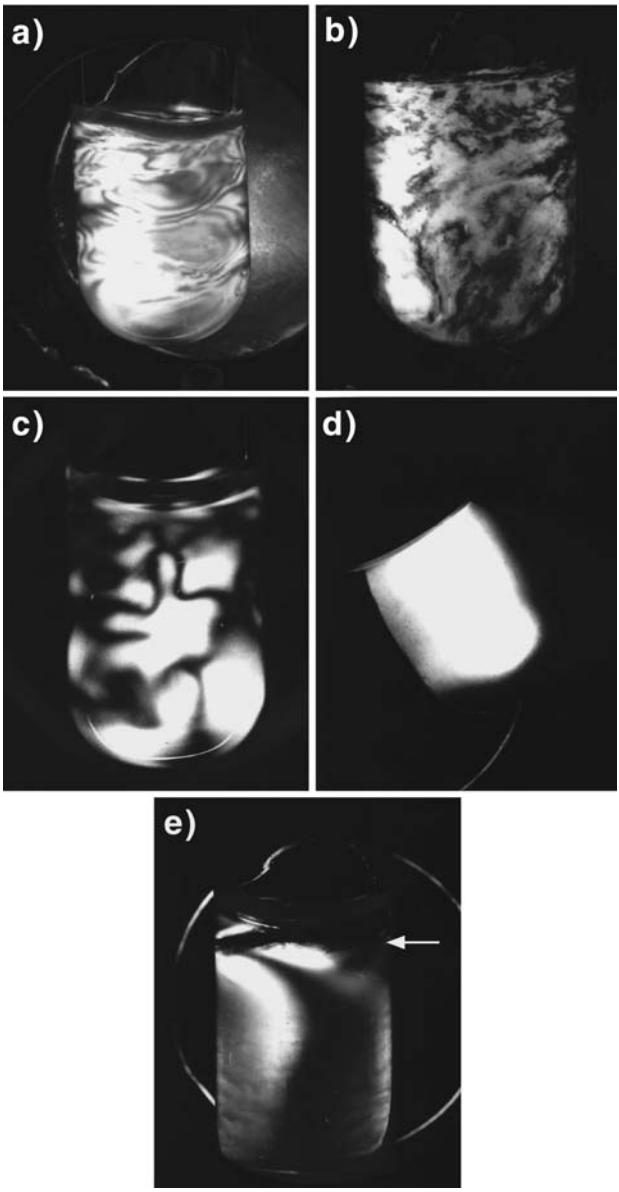


**Fig. 10a–e.** Tubes of aqueous clay suspensions observed between crossed polarizers: **a** bentonite suspensions of concentration 0.043 g/cm$^3$; **b** laponite suspensions of concentration 0.043 g/cm$^3$; **c** flow birefringence in a bentonite suspension of concentration 0.019 g/cm$^3$ – the test tube was previously vigorously shaken and was photographed during relaxation; **d** example of an oriented laponite suspension over a centimeter length scale – the sample looks bright because its principal axes are close to 45° with those of the polarizers; **e** an initially isotropic sample of bentonite gel (c=0.020 g/cm$^3$, bottom) in contact with brine (5 mol/l) turns birefringent. The *arrow* points to the interface between the gel and the brine. (Reprinted from [4b], copyright (2000) from John Wiley and Sons)

crease over many years. This means that, at least during the first weeks, the particles are not completely frozen and that any accidental flow birefringence could in fact relax. Third, birefringent gels may be prepared in test tubes by slowly concentrating isotropic sols over weeks. This process does not involve any flow. In this way, nematic single domains as large as a cubic centimeter were reproducibly prepared (Fig. 10d). Moreover, birefringence appears at the same concentration as that determined on samples prepared in the usual way. Then, the mechanical history of the sample seems irrelevant in this respect. Therefore, these studies show that a nematic order prevails in these suspensions over a distance that can be as large as 1 cm. Nevertheless, this discussion not only emphasizes that one should not confuse plain flow birefringence with true nematic ordering but also illustrates the difficulties of working with gels.

Very recently, well-aligned samples of laponite gels (c=0.02 g $cm^{-3}$) were prepared by slowly concentrating isotropic sols directly in Lindemann glass capillary tubes suitable for SAXS experiments, instead of test-tubes as described in the previous paragraph. The SAXS patterns observed are clearly anisotropic (Fig. 11a), which demonstrates the nematic orientational order at the particle scale over the whole sample [52]. Moreover, the SAXS patterns also show that the positional correlations of the clay particles are very weak, which is a well-known feature of these laponite gels [53]. This allows one to model easily the SAXS pattern (Fig. 11b) by only considering the particle form factor and the Maier-Saupe orientational distribution function that classically describes the nematic order [1]. By fitting the SAXS pattern, the nematic order parameter is obtained, S=0.55±0.05. This value compares quite well with those of usual liquid crystals (0.4–0.8) and shows that the nematic order of these materials should always been kept in mind when elaborating experimental procedures.

The phase diagram of these suspensions has been established versus clay volume fraction and ionic strength (Fig. 12) allowing the behavior of the sol-gel as well as the isotropic-nematic phase transitions to be followed. At high salt concentration (>0.3 mol $l^{-1}$ for bentonite and >$9\times10^{-3}$ mol $l^{-1}$ for laponite), the repulsive electrostatic interactions are screened sufficiently so that short-range attractive interactions can take over inducing the flocculation of the suspension. Very strikingly, in the case of bentonite (Fig. 12a), the nematic phase is stabilized upon increasing the ionic strength: an increase of the ionic strength induces both gelation and the isotropic-anisotropic phase transitions to occur at lower clay concentration. If one follows a vertical line on this diagram, and for example starts with a liquid suspension of bentonite (1.5 wt%) in pure water, at a concentration of [NaCl]=0.02 mol $l^{-1}$ the suspension is an isotropic gel and at [NaCl]=0.1 mol $l^{-1}$ it is a birefringent gel. Therefore, adding some brine on an isotropic gel of bentonite of concentration slightly under the isotropic/nematic transition allows one to induce the phase transition without any slightest flow, another hint at the thermodynamic origin of this transition (Fig. 10e). This effect, though unexpected, was still predicted by a statistical physics model incorporating electrostatic interactions [54]. Furthermore, a similar phase diagram was recently reported by Mourchid and Levitz on a closely related form of laponite, in a thorough and detailed study [55]. The same authors have fully discussed the relation between gelation and nematic ordering in this system. They

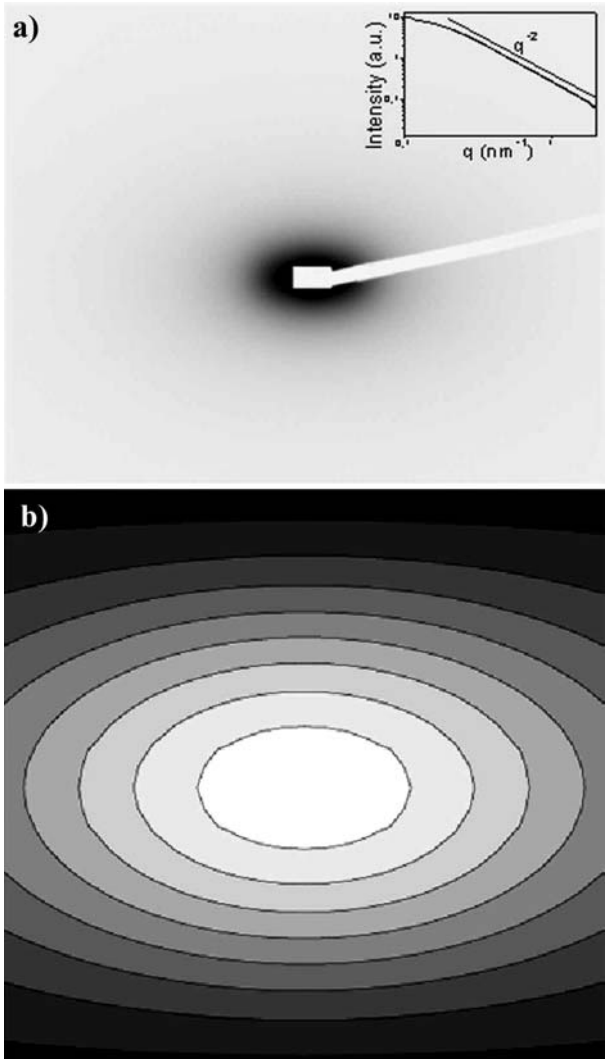


**Fig. 11.** **a** Anisotropic SAXS pattern of an aligned sample of clay gel in a horizontal capillary. Insert: SAXS intensity vs scattering vector modulus of an unoriented sample of the same concentration. (The *straight line* shows the $q^{-2}$ dependence typical of the "intermediate regime" of plate-like particles). **b** Calculation of the SAXS pattern, with L=1 nm, R=15 nm, and S=0.55, that gives good agreement with the experimental one. (Reprinted from [52], copyright (2002) from EDP Sciences)

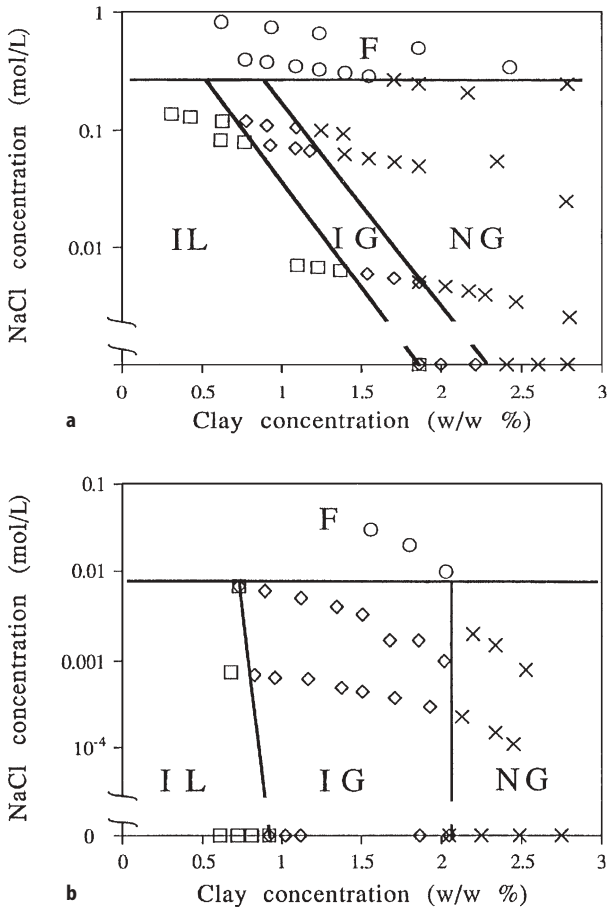


**Fig. 12a,b.** Phase diagram of clay suspensions vs clay and NaCl concentrations. (*circles*, F) Flocculated samples; (*squares*, IL) isotropic liquid samples (*lozenges*, IG) isotropic gel samples; (*crosses*, NG) nematic gel for: **a** bentonite; **b** laponite. (Reprinted from [4b], copyright (2000) from John Wiley and Sons)

have also explored the phase diagram at very low ionic strength and found the existence of a soft solid stabilized by long-range electrostatic repulsions [56].

In addition, it should be noted that there is now quite a few experimental studies that directly or indirectly document the existence of nematic order in clay gels [57]. Among them, let us particularly mention the direct visualization of aligned domains by X-ray fluorescence microscopy [58]. These clay-rich domains may arise from the nematic/isotropic phase separation that takes place at the micron length scale but does not extend to the macroscopic scale due to gelation, as discussed above. Another recent study leads to very similar conclusions [59]: Magnetic spherical colloidal particles of maghemite were incorporated as probes into laponite gels. A microscopic phase separation was also observed in

the region of the phase diagram where the nematic/isotropic phase separation was expected. Finally, all these various studies raise the same and yet open question: what is the interplay (if any) of the nematic/isotropic phase transition with the gelation of these clay suspensions [60]?

### 4.2 A Unique Liquid-Crystalline Lamellar Phase Comprised of Mineral Nanosheets: $H_3Sb_3P_2O_{14}$

Until very recently, a liquid-crystalline lamellar phase based on extended, covalent, solid-like sheets had never been reported, even in the huge field of organic lyotropic phases. However, the field of mineral compounds provides a wealth of original moieties that are not usually obtained from organic synthesis techniques. Any general chemistry textbook will show a wealth of low-dimensionality mineral compounds and among them, many are two-dimensional ones. The problem then is to try to disperse them in a suitable solvent without alteration. We have already discussed in a previous section the principles that lead to the successful dispersion of mineral moieties and this approach will be further illustrated with the following example [61]. The members of the series of solid acids $H_nM_nZ_2O_{3n+5}$ (with, for example, M=Sb, Nb, Ta; Z=P, As; n=1, 3) are known to display a crystalline lamellar structure [62][2]. Among them, $H_3Sb_3P_2O_{14}$ was found to disperse fully in water to yield homogeneous, transparent, colorless suspensions of extended covalent sheets of 1 nm thickness and at least 300 nm in diameter. The observation (Fig. 13) in polarized light of a series of test-tubes

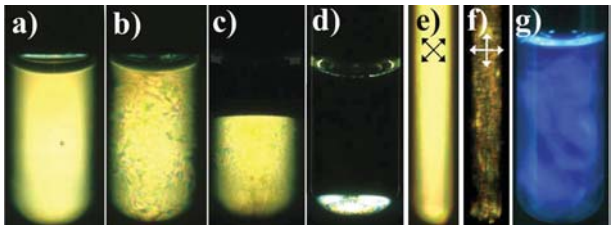


**Fig. 13a–g.** Naked-eye observation of samples. Test-tubes filled with aqueous suspensions of $H_3Sb_3P_2O_{14}$ single-layers, observed between crossed polarizers (a–e) (the isotropic phase appears dark): **a** 2 ml of birefringent gel phase ($\phi$=1.98%) (topological defects are so dense that the texture appears homogenous at the scale of this photograph); **b** 2 ml of birefringent fluid phase ($\phi$=0.93%); **c** 2 ml of a biphasic sample with an overall volume fraction $\phi_o$=0.65%; **d** 2 ml of a biphasic sample with an overall volume fraction $\phi$=0.03%; **e, f** magnetically aligned sample observed in a 5-mm NMR tube that has been immersed 10 min in a 18.7 T field at 50 °C, in two different orientations compared to the polarizer/analyzer system represented by *arrows* ($\phi$=0.75%); **g** sample iridescence ($\phi$=0.75%) observed in natural light and due to light scattering by the $H_3Sb_3P_2O_{14}$ layers stacked with a period of 225 nm. (Reprinted by permission from Nature [61], copyright (2001) Macmillan Publishers Ltd)

[2] In some cases, test tubes have shown temporarily a rainbow set of colors (see www graphical abstract) (induced by strong centrifugation for example), prior to reaching a single color equilibrium state.

filled with suspensions of decreasing volume fractions shows that: i) samples of high volume fractions ($\phi$>1.78%) form birefringent gels; ii) for 1.78%>$\phi$ > 0.75%, the samples form a fluid birefringent phase; iii) for 0.75%>$\phi$, the suspensions demix into a bottom birefringent fluid phase and a top isotropic one.

SAXS experiments (Fig. 14) have proved that the birefringent phase (sol and gel) has a lamellar structure and that its period can be continuously tuned from 1 to 225 nm according to dilution. In fact, very dilute samples are iridescent because the lamellar structure then has a period comparable to the wavelengths of visible light [62]. A large number (up to 10) of lamellar reflections were observed by SAXS, even at high dilutions, which shows the strength of the interactions between the mineral sheets. Further dilution leads to phase separation as excess water is expelled from the lamellar phase. Adding salt destabilizes the liquid-crystalline phase, eventually leading to flocculation of the colloid, indicating that these interactions are most probably of an electrostatic nature; this is hardly surprising as the sheets bear a rather large electrical charge. In addition, wide-angle X-ray scattering experiments have revealed the existence of sharp diffrac-

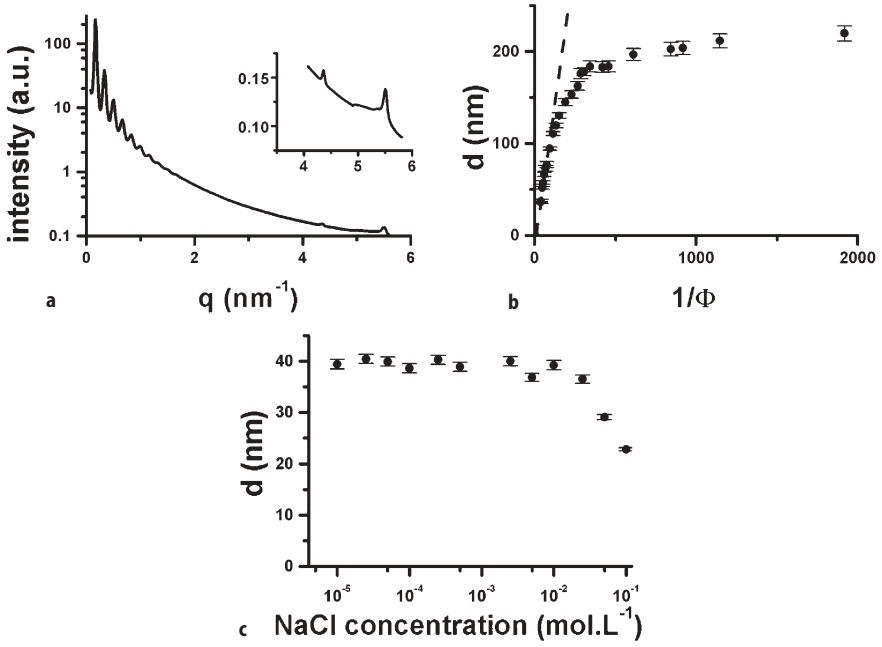


**Fig. 14a–c.** USAXS study of "powder" samples: **a** an example of scattered intensity vs scattering vector modulus q, showing ten orders of reflection due to the lamellar period as well as, in the inset, the thin diffraction lines due to the two-dimensional positional order within the covalent layers ($\phi$=2.0%); **b** variation of the lamellar period, d, with inverse volume fraction (including two data points at very small d extracted from [62]) – the *dashed straight line* represents the one-dimensional swelling behavior of the lamellar phase d=$\delta/\phi$ with $\delta$=1.05 nm. A crossover from this law to a plateau is observed when entering the biphasic regime; **c** variation of the lamellar period d with salt molarity at constant volume fraction ($\phi$=1.9%). (Reprinted from [61], copyright (2001) from Nature Publishing Group)

tion lines due to the crystalline order within the mineral sheets that do not fold or crumple but are fully preserved in suspension.

The mineral lamellar phase is readily aligned by shear in a Couette cell (Fig. 15) and the covalent sheets align parallel to the shearing surfaces. Dilute samples could be aligned at rather low shear rates (30 $s^{-1}$) and showed the best orientations. Moreover, the mesophase also aligns in high magnetic fields with the sheets perpendicular to the field, which provides a simple way to produce large (centimetric) oriented lamellar samples. This property was exploited by using the lamellar phase as a medium to induce a weak alignment of biomole-

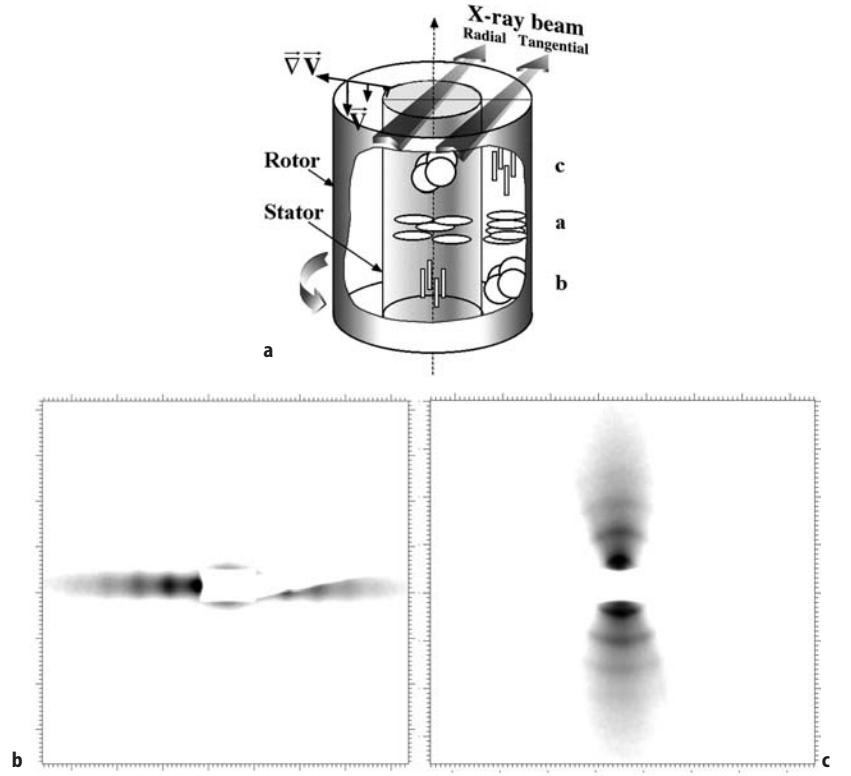


**Fig. 15a–c.** USAXS studies of aligned samples: **a** scheme of the Couette shear cell illustrating the radial and tangential geometries with respect to the X-ray beam (*flat arrows*). We also depict within the cell the three different types of lamellar orientations (a, b, and c) as seen by the X-rays in both geometries (the layers are sketched as *circular disks*); **b** USAXS 2-D scattering pattern obtained with a sample aligned in a Couette shear cell, in the tangential geometry, showing that the layers (d=175 nm) mostly belong to the c orientation; **c** USAXS 2-D scattering pattern of a vertical capillary filled with a suspension of $H_3Sb_3P_2O_{14}$ ($\phi$=0.75%), obtained 20 min after its alignment using an 18.7-T magnetic field applied along its long axis. The vertical localization of the interference peaks (d=215 nm) indicates that the layers are oriented perpendicular to the magnetic field (in this case, since no mechanical shear is applied, the sample relaxes back to a powder within 1–2 h once removed from the magnetic field). (Reprinted from [61], copyright (2001) from Nature Publishing Group)

cules, which proves helpful when trying to determine their structure by NMR (see Sect. 6, Emerging Fields section).

## 5
## Anisotropic Nanoparticles

### 5.1
### Boehmite, a Model System to Test the Onsager Theory

The boehmite system ($\gamma$-AlOOH), originally studied by Zocher and Torök [63] and Bugosh [64] was further developed by Lekkerkerker and coworkers [65]. They extended the hydrothermal preparation pioneered by Bugosh [64] by starting from an aqueous aluminum alkoxide mixture acidified with hydrochloric acid [65a]. They studied the phase behavior of both charge stabilized aqueous dispersions of colloidal boehmite rods [65b,c] as well as sterically stabilized colloidal boehmite rods in an organic solvent (cyclohexane) [65d–f].

Using the aqueous suspensions as obtained from the hydrothermal treatment, the I–N transition was observed, but took a very long time (months) [65b]. On the other hand, by treating the boehmite dispersions with hydrolyzed aluminum polycations, the phase transition is complete in a few days [65c]. In retrospect, it appears that the boehmite suspensions prepared by Bugosh also contain aluminum polycations. The sterically stabilized boehmite dispersions undergo the I–N phase transition. The biphasic gap is much wider than predicted by the Onsager theory for a monodisperse sample [65e], but can be explained by taking into account the polydispersity [65f]. The rate of the I–N transition strongly depends on the concentration. Upon increasing concentration from $c_i$ to $c_n$, polarization microscopy indicates a crossover from nucleation and growth to spinodal decomposition [66].

At this point, let us detail the conditions of validity and the main predictions of the Onsager theory. This model applies to very anisotropic rod-like (or disk-like) particles. An important quantity is the particle aspect ratio, L/D, defined as the ratio of its length L over its diameter D. The particles should only interact through a purely hard-core potential, which means that particles do not interact at all if they do not touch, but they also cannot interpenetrate each other. This statistical physics model is based on a balance of two kinds of entropies. As concentration of rod-like moieties increases, the system undergoes nematic ordering because its loss of orientational entropy is more than compensated by a gain in translational entropy. The predictions of the model are the following. The nematic/isotropic transition should be first-order, i.e., with phase coexistence. The concentrations of the coexisting nematic and isotropic phases are given by $c_n$=4.2D/L and $c_i$=3.3D/L respectively. The nematic order parameter should jump from 0 to 0.8 at the transition. Temperature has no effect on this transition and the system is called athermal. Thus, the predictions of the Onsager model and of more recent theories based on it were confirmed by the detailed and precise investigations using the suspensions of grafted boehmite rods dispersed in cyclohexane. Figure 16 illustrates the first-order nematic/isotropic phase transition of these grafted boehmite rods. The effect of controlled polydispersity was

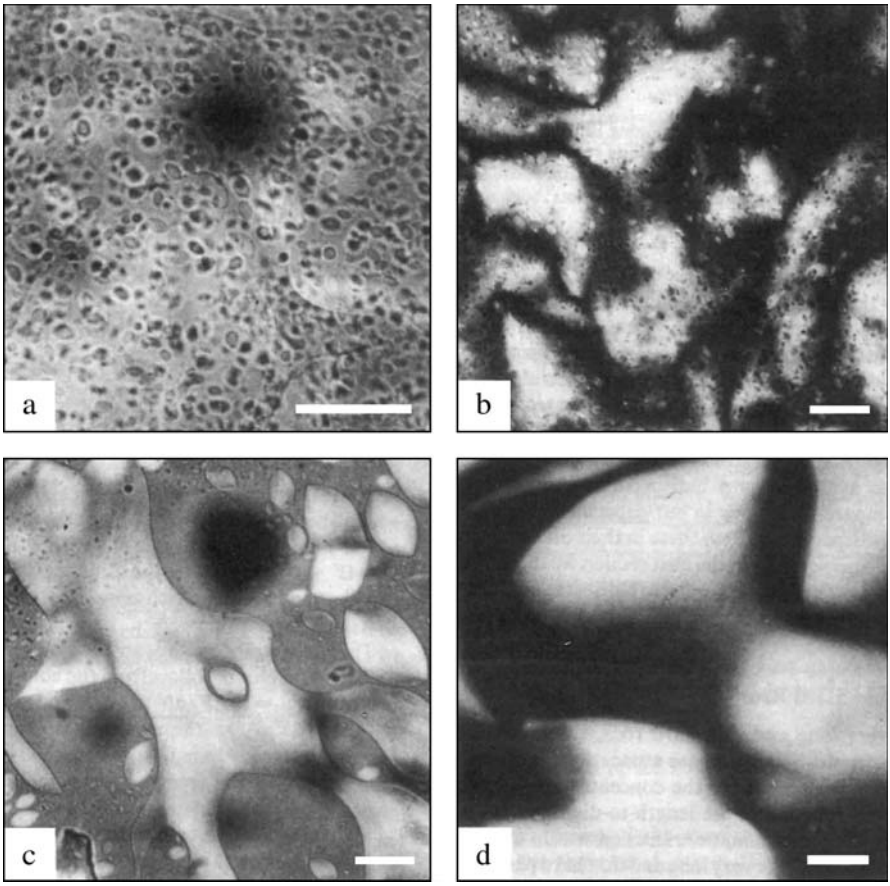


**Fig. 16.** **a** Optical micrograph of the nucleation of very small nematic droplets. **b** Nematic droplets and underneath a continuous nematic lower phase with Schlieren. **c** Grown-out tactoids. **d** Schlieren texture after completion of phase separation. All observations with crossed polarizers. The length of the *bar* represents 20 μm (Reprinted from [65e], copyright (1993) from the American Chemical Society)

also examined and the complex coexistence of two different nematic phases with the isotropic liquid phase, which is a consequence of polydispersity predicted by theory, was proved experimentally.

Non-grafted boehmite rods experience a much more complicated interaction potential as positive surface electrical charges now play an important role. In this case, the phase diagram has to be discussed in the frame of both the Onsager model of nematic ordering and the DLVO (named after: B.V. **D**eryagin, L. **L**andau, E.J.W. **V**erwey, and J.T.G. **O**verbeek) theory of colloidal stability, which describes colloidal stability as a balance between repulsive electrostatic and attractive van der Waals interactions [67, 68]. At low ionic strength, electrostatic repulsion dominates so that the phase stability is essentially described by the

Onsager model. However, at large ionic strength, these electrostatic repulsions are screened and van der Waals attractions come into play. Indeed, the strength of these latter interactions depends through the Hamaker constant on the electronic contrast between the mineral moieties and the solvent. Mineral moieties being electron rich are likely to show a large Hamaker contrast with the solvent. In the case of boehmite rods, these strong van der Waals attractions lead to the formation of dense space-filling isotropic gels. It should be noted at this point that the percolation threshold of very anisotropic rods is inversely proportional to their aspect ratio so that gels can be formed at rather low volume fractions. Note that a rather similar situation also prevails for the aqueous dispersions of $V_2O_5$ ribbons [69].

The same authors also investigated the dynamic properties of these suspensions by light scattering and rheology both in the isotropic liquid phase and in the nematic one. Even though this constitutes one of the most comprehensive studies of its kind for suspensions of rod-like moieties, we shall not further discuss their findings, as they are well described [68, 70].

### 5.2
### Gibbsite and the Onsager Transition for Disks

In his seminal work of 1948, Onsager had already predicted the existence of a nematic phase for suspensions of disk-like particles. However, it was only fifty years later that Van der Kooij and Lekkerkerker clearly proved this conjecture by carefully investigating suspensions of gibbsite, $Al(OH)_3$, hexagonal platelets [71]. These particles were sterically stabilized by grafting them with a layer of polyisobutene before being dispersed in toluene. The aspect ratio of these moieties, defined as the ratio of their diameter (≈170 nm) to their thickness (≈15 nm), is approximately 11. In a given range of volume fraction (0.16–0.17), these suspensions spontaneously phase separate (Fig. 17) into a nematic and an isotropic phase as predicted by Onsager, and also more recently confirmed by computer simulations [72]. The birefringent nematic phase, being denser than the isotropic one, sediments at the bottom of the tube. Moreover, the relative proportion of the nematic phase increases linearly with the gibbsite volume fraction, as expected (Fig. 17a–d). The isotropic upper phase shows streaming birefringence when the tube is slightly shaken, indicating the presence of free alignable platelets. The lower phase is permanently birefringent due to nematic ordering and flows like a moderately viscous liquid when the tube is tilted, both properties proving its liquid crystalline nature. This phenomenon proves that the nematic order of gibbsite suspensions of volume fraction larger than 0.17 is really of a thermodynamic nature. In addition, the range of volume fraction of the biphasic gap is in relatively good agreement with the theory. This experimental study also proves that grafting particles with a polymer layer ensures that they strictly interact through a hard-core potential. Indeed, the thickness of the polymer layers prevents the particles from approaching each other at short range where electrostatic and van der Waals interactions come into play.

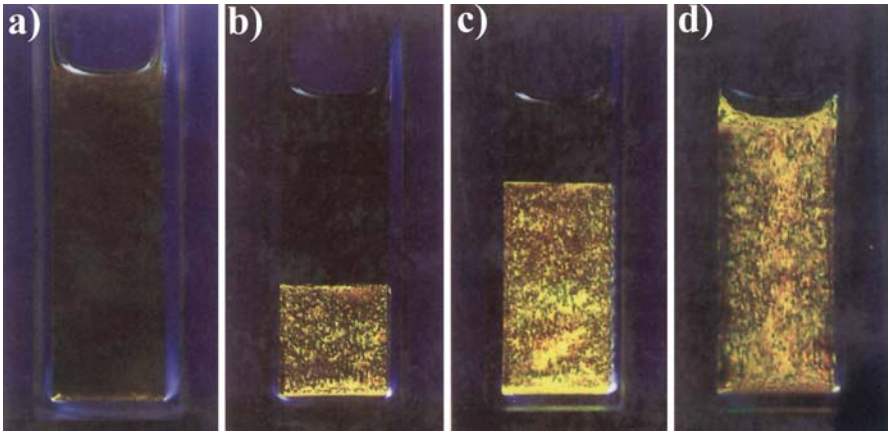


**Fig. 17a–d.** Isotropic-nematic phase separation as observed between crossed polarizers, at volume fractions ranging from; **a** 15.9; **b** 16.5; **c** 16.9; **d** 17.4 vol.%. (Reprinted from [71], copyright (1998) from the American Chemical Society)

## 5.3 Liquid Crystalline Hexagonal Phase of Disks: $Ni(OH)_2$

Liquid crystalline phases can show not only long-range orientational order as nematic phases do but also long-range positional order. When this positional order is one-dimensional, the mesophase is called lamellar or smectic; when it is two-dimensional, it is called columnar. The latter case is often found with thermotropic liquid-crystal disk-like molecules. Such molecules stack in columns that assemble on a 2-D lattice of hexagonal, rectangular, or oblique symmetry. The molecules in a given column only show 1-D liquid-like order and the uncorrelated columns are free to slide past each other, which ensures the mesophase fluidity [73].

Very recently, a hexagonal columnar mesophase has been reported in two different mineral systems. In the first example, nickel hydroxide ($Ni(OH)_2$) hexagonal plate-like particles have been grown by controlled precipitation [74]. They were then coated with a polyacrylate layer in order to avoid flocculation by steric repulsion. The bare particles are about 90 nm in diameter and about 10 nm thick, with an aspect ratio of 9:1. The polymer layer being about 4 nm thick, the particles, when coated, have an aspect ratio of about 5:1. The nickel hydroxide particles are charged and the strength of the electrostatic interactions can be tuned by adding salt. Observations of macroscopic samples with the naked eye, in polarized light, show, in a given range of concentration, the coexistence of two phases – a top isotropic phase and a bottom birefringent one. Small Angle Neutron Scattering (SANS) experiments on "powder" (i.e., unoriented) samples displayed five diffraction peaks. The first two, located at small scattering angles, in a ratio $1:3^{1/2}$, suggest the existence of a two-dimensional hexagonal lattice whereas the last three, located at wider angles, in a ratio 1:2:3, correspond to the stacking of the plates in columns. Very interestingly, this mineral phase looks therefore quite similar to the hexagonal columnar mesophase of usual disk-like organic mole-

cules. This interpretation was further confirmed by detailed SAXS experiments on aligned samples [75] and the experimental phase diagram was compared to that predicted by computer simulations for plate-like particles [76]. This system also allows one to balance delicately electrostatic and steric interactions by the control of the ionic strength, a possibility that was explored to some extent by the authors. The flow properties of this hexagonal phase, upon shear in a Couette cell, were also investigated [77]. It was found that, at low shear rates, the phase is aligned with columns in the flow direction but the particles have their normals tilted by 20° with respect to the flow direction. As the shear rate is increased, a kind of dynamical transition is observed to a layered state in which the layers and the particles are oriented with normals parallel to the shear gradient. The kinetics of alignment and relaxation were also investigated in detail.

The second example is found in the system of gibbsite disks that we already described in a previous section. In fact, this system shows not only an isotropic/nematic phase transition at a volume fraction of about 20% but also a nematic/columnar phase transition at around 40% [78]. The hexagonal phase is similar in nature to that of the $Ni(OH)_2$ particles but this system provides the additional opportunity to investigate the influence of polydispersity, a parameter that often plays a major role in determining whether a given phase will actually be observed. Two gibbsite systems were prepared that differ by their polydispersities. It was first found in the two systems that the coexisting nematic and columnar phases had different polydispersities. The columnar phase has a markedly smaller polydispersity than the nematic one so that the phase transition could be used to improve the size distribution of a suspension. It was then observed that, in the system of higher polydispersity, the hexagonal phase seemed to be replaced by a lamellar one at higher volume fraction. This nicely illustrates the disruptive effect of the diameter polydispersity, an effect that was indeed awaited. In fact, the relative stability of the nematic, columnar, and lamellar phases are not only controlled by the volume fraction but also by a subtle balance between plate diameter and thickness polydispersities.

Suspensions of colloidal gibbsite platelets of very large thickness polydispersity but of rather monodisperse diameter display a very unusual phenomenon [79]. In a limited range of volume fraction, these suspensions demix into a nematic *upper* phase in coexistence with an isotropic *bottom* phase. This is in stark contrast with the usual case where the nematic phase is denser than the isotropic one. This behavior was interpreted as due to a fractionation effect related to the strong thickness polydispersity as the thicker platelets are largely expelled from the nematic phase and preferentially occupy the isotropic phase. Note that a theoretical model was especially developed in order to account for these quite peculiar observations [80]. Moreover, this model predicts that the nematic phase may demix into two separate nematic phases of differing densities and compositions.

### 5.4
### Mixtures of Rods and Plates

The liquid crystalline behavior of mixtures of rod-like and plate-like particles is intrinsically much richer than those of rods and plates considered separately.

This is nicely illustrated by mixing the suspensions of goethite rods and gibbsite plates already described in this review. One of the motivations to undertake this kind of study was to find a new type of nematic phase, called biaxial [1]. Even though this biaxial nematic was not found here, the mixtures do present a remarkably rich phase diagram with four different liquid crystalline phases [81]. Up to five phases coexist in a region of the phase diagram. Two of these mesophases are nematic but are rod-rich and plate-rich respectively, another one is the columnar phase already described above, the nature of the fourth mesophase is still unknown, and the last phase is the isotropic one. The observation of a five-phase equilibrium region implies that the phase diagram cannot be explained without explicitly taking into account the polydispersity of both rods and plates. Actually, the two nematic phases differ not only in rod/plate proportion but also in particle dimensions. Strong fractionation effects also occurred in the columnar phase, resulting in a more pronounced columnar ordering than observed with suspensions of plate-like particles only. A theory adapted from the Onsager model was successfully developed to account for the corner of the phase diagram that shows the isotropic phase, the rod-rich and plate-rich nematic phases, and all the possible equilibria between them [82]. Finally, it was observed that the formation of the rod-rich nematic phase proceeds by the mechanism of spinodal decomposition whereas that of the plate-rich nematic phase proceeds by a nucleation-growth process [83].

### 5.5
### $\beta$-FeOOH, a Colloidal Smectic Phase

In his search for ordering phenomena in suspensions of mineral crystallites, Zocher and Jacobsohn observed, in 1929, iridescent layers at the bottom of a flask filled with a colloidal solution of $\beta$-FeOOH (akaganeite) [84]. He called these layers "Schiller layers", which means iridescent layers in German. $\beta$-FeOOH forms fairly well monodisperse nanorods 500 nm long and 100 nm in diameter. The iridescence is due to the sedimentation of these rod-like particles, which form layers at the bottom of the flask [85]. The thickness of each layer, roughly the particle length, is comparable to the wavelength of light, explaining the iridescence. A lamellar structure is thus formed which is similar to the molecular organization of thermotropic smectic phases, but here the periodicity is about 100 times larger. This colloidal liquid crystalline phase coexists with the supernatant phase, which is a dispersion of individual rods. The thermodynamics of this phase transition could also be understood in the frame of the DLVO theory. Again, temperature has very little influence on the phase stability, pointing to a purely steric potential. Moreover, detailed studies [86] of dried Schiller layers by atomic force microscopy has shown that the layers can have two types of internal structure: the rods can pack on a distorted square lattice and be tilted with respect to the layer normal or they can assume a liquid-like ordering within the layers. Similar phenomena seem to exist in suspensions of tungstic acid, but they are less well documented. Finally, this example proves that very monodisperse mineral particles can form a colloidal smectic phase.

### 5.6
### Suspensions of Goethite Nanorods

Goethite ($\alpha$-FeOOH), which should not be confused with akaganeite ($\beta$-FeOOH), is one of the most widespread iron oxides [87]. It is widely used as a pigment in industry. Aqueous suspensions of goethite nanorods are readily obtained by raising the pH of an aqueous $Fe(NO_3)_3$ solution. The resulting precipitate is aged at room temperature, centrifuged, and rinsed several times, and finally dispersed at pH 3. At this pH, which represents a compromise between chemical and colloidal stabilities, due to the large surface charge density (0.2 C $m^{-2}$), electrostatic interactions prevent flocculation. The nanorods are strongly polydisperse with average length of 150 nm, width of 25 nm, and thickness of 10 nm. Goethite suspensions display a liquid crystalline phase at volume fractions of approximately 10%.

Despite the fact that bulk goethite is a typical antiferromagnet, the nematic suspensions of goethite nanorods display quite unexpected magnetic properties [88]. For instance, they align in very weak magnetic fields as the alignment (Frederiks) transition takes place at 20 mT for samples 20 μm thick. This field intensity is at least an order of magnitude smaller than observed in usual thermotropic and lyotropic liquid crystals. This mineral liquid crystal is therefore extremely sensitive to a magnetic field. Moreover, nematic suspensions of

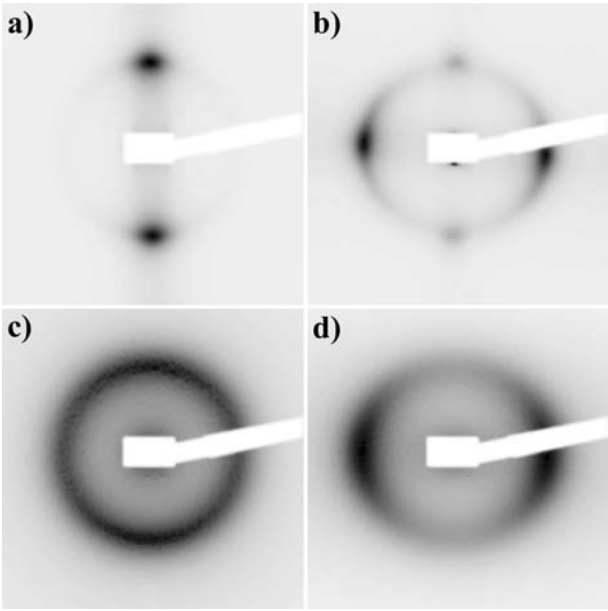


**Fig. 18a–d.** SAXS patterns of: **a** a nematic phase sample in a 30-mT field; **b** a nematic phase sample in a 625-mT field; **c** an isotropic phase sample in a 270-mT field; **d** an isotropic phase sample in a 900-mT field. (Reprinted from [88], copyright (2002) from the American Physical Society)

goethite align parallel to the field at low field intensities (≤350 mT) but, oddly enough, they reorient perpendicular to the field at large field intensities (≥350 mT) (Fig. 18). This behavior is again in sharp contrast with those of usual liquid crystals that align, at all field intensities, either parallel or perpendicular to the field, depending on their nature. It should also be noted that this property is also observed with initially isotropic goethite suspensions that show huge magnetic-field induced anisotropies and orientation reversal around 350 mT as well. Then, this phenomenon simply reflects the individual properties of the nanorods, even though they are probably enhanced by collective effects in the nematic phase. These quite peculiar magnetic properties probably arise from a competition between a nanorod remanent magnetic moment due to uncompensated surface spins and a negative anisotropy of its magnetic susceptibility.

## 6
## Emerging Fields

### 6.1
### Self Assembly of Nanorods and Nanowires

In the recent past, and following the discovery of nanotubes by Iijima [89], there has been an enormous increase in the number of groups and reports concerning the synthesis of nanorods, nanowires, as well as nanotubes. Most of the elements of the periodic table have now been used (N.B. the difference between nanorods and nanowires is that nanorods usually have a small aspect ratio when nanowires have a high one). These particles, which present a wide range of properties such as semiconducting or metallic behavior, could lead to numerous new liquid crystalline phases and by clever exploitation of their self-assembly properties, numerous new materials with a variety of applications could be synthesized. Since the number of such phases is increasing so rapidly, we have summarized the most studied systems and what we consider to be the most original in Table 1, although we must add that this is not an exhaustive list.

#### 6.1.1
#### *Synthesis*

Dozens of methods to synthesize nanotubes, nanowires, and nanorods have been reported that can be found in the references included in Table 1. In addition to the most well known ones, such as hot plasmas, laser ablation, chemical vapor deposition, high temperature solid state and hydrothermal synthesis, filling/coating of carbon nanotubes and similar types of materials, three methods have been developed that enable the synthesis of a wealth of new anisotropic nanoparticles.

The first one makes use of the pores of membranes as templates for the electrolytic growth of metal nanorods. This technique consists of coating one side of a membrane with a metal electrode (such as gold or platinum) and then electrodepositing a metal or conducting polymer within the pores of the membrane [90]. This method controls more closely the filling of the pores compared to other

**Table 1.** A selection of the most common or original nanotubes, nanorods, and nanowires and their method of synthesis [131]

| Composition | Synthesis method(s) | Type | Reference |
|---|---|---|---|
| C | Arc, laser ablation, CVD, templating etc. | NT | [98a, 130] |
| Ag | AAO templating | NW, NR | [131] |
| Au | AAO templating | NW, NR | [132, 133] |
| Bi | AAO templating | NW | [134] |
| C (diamond) | AAO templating | NW | [135] |
| Co | AAO templating | NW | [136, 137] |
| Cu | AAO templating | NW, NR | [95, 138] |
| Fe | AAO templating | | [139] |
| Ni | AAO templating | | [137] |
| Ge | Laser ablation | | [140] |
| Si | Laser-assisted catalytic growth, laser ablation, catalytic growth, HT synthesis, thermal evaporation SiO, CVD | | [141, 142] |
| Vanadium oxides($V_2O_5$, VOx, $Na_2V_3O_7$) | Solution, hydrothermal, NT AAO templating, others | NT, NR | [143–145] |
| $TiO_2$ | AAO templating, self assembly, sol-gel, wet chemistry | NT, NW | [144, 146, 147] |
| $SnO_2$ | AAO templating | NW | [10, 148] |
| $Al_2O_3$ | Anodisation | NT, NW | [141, 149] |
| $In_2O_3$ | AAO templating | NW | [150] |
| ZnO | AAO templating, PVD | NW | [144, 147, 151, 152] |
| $WO_3$ | AAO templating, NT templating | NW, NR | [144, 146, 147] |
| $SiO_2$ | AAO templating (mesoporous), templated coprecipitation, wet chemistry, laser ablation, carbothermal reduction, sol-gel | NT, NW | [144, 153] |
| $Co_3O_4$ | AAO templating, | NW | [144] |
| $MnO_2$ | AAO templating, | NW | [144] |
| $MoO_3$ | NT templating | NT, NR | [145] |
| $Sb_2O_5$ | NT templating | NT, NR | [145] |
| $MoO_2$ | NT templating | NT, NR | [145] |
| $RuO_2$ | NT templating | NT, NR | [145] |
| $IrO_2$ | NT templating | NT, NW | [145] |
| $Ga_2O_3$ | High T, arc discharge, carbothermal reduction | NW | [152, 154] |
| CuO | Solid state (grinding) | NR | [155] |
| $\alpha$-$Fe_2O_3$ | Controlled precipitation | NR | [156] |
| BaCrO4 | Reverse micelle templating | NW | [96] |

**Table 1** (continued)

| Composition | Synthesis method(s) | Type | Reference |
|---|---|---|---|
| $BaWO_4$ | Reverse micelle templating | NR | [157] |
| $YBa_2Cu_3O_7$ | Laser ablation | NR | [158] |
| $MoS_2$ | Catalyzed transport reaction, $H_2$ reduction, C60 and CNT templating, other | NT | [159–161] |
| $WS_2$ | $H_2$ reduction of $WS_3$, $WO_x$+$H_2S$, other | NT | [160–162] |
| $WSe_2$ | HT reaction | NT | [163] |
| $W_xNb_yS_2$ | HT reaction | NT | [164] |
| $W_xMo_yC_zS_2$ | $W_xNb_yO_z$+$H_2S$ | NT | [165] |
| $NbS_2$ | $H_2$ reduction of $NbS_3$ | NT | [166] |
| $TaS_2$ | $H_2$ reduction of $TaS_3$ | NT | [166] |
| $FeTe_2$ | Hydrothermal | NR | [167] |
| $SiSe_2$ | Theoretical study | NW | [168] |
| $Bi_2Te_3$ | AAO templating | NW | [169] |
| $LiMo_3Se_3$ | HT synthesis+cation exchange | NW | [13, 170] |
| $NaNb_2PS_{10}$ | HT synthesis | Nanotubules | [34] |
| $Cu_2S$ | Cu (surfactant treated)+$H_2S$ | NW | [171] |
| ZnS | HT conversion of ZnO | NR | [172] |
| CdS | Thermal decomposition | NR, NW | [173] |
| CdSe | AAO templating | NR, NW | [97, 174] |
| BN | Arc, laser ablation, CVD, templating etc. | NT | [175–180] |
| GaN | Use of growth promoter, CNT templating | NW | [152, 181] |
| AlN | HT synthesis | NW, NR | [152] |
| SiN | Si-$SiO_2$+$N_2$+2C (CNT templating) | NR | [182] |
| InP | Laser-assisted catalytic growth | NW | [183] |
| GaAs | Laser-assisted catalytic growth, laser ablation | NW | [184, 185] |
| SiC | Arc, HT reaction via CNT templating, carbothermal reduction, HFCVD | NW, NR | [186] |
| TiC | HT reaction | NW | [187] |
| MC (M=transition metals, Ge, Ta, Gd, Hf, La) | Various | NR | [188] |

nanometer sized materials that have been used, such as the pores of membranes, zeolites, or mesoporous materials [91]. It even allows one, by changing the voltage during the electrodeposition, to synthesize nanowires made of periodically alternating metals [92]. Note that these "striped" metal nanoparticles, in which the stripes are comprised of different metals such as gold, silver, platinum, and nickel, can be visualized using bright-field optical microscopy, which allows them to be used as nano-barcodes [93]. Indeed, in an analogous fashion to conventional barcoding, this technology enables the creation of an extremely large numbers of unique and identifiable particles by varying the width and composition of the stripes. Individual particles can be identified by reading the striped pattern using an optical microscope. Nanobarcoded particles can be used to carry out simultaneously large numbers of biological assays in a small volume.

The second approach takes advantage of tools developed in the field of "*Chimie douce*" typically applied for synthesizing metal nanoparticles, semiconductors or oxides. By analogy to biomineralization, in which minerals are induced to form within an isolated space (a cell or a cell compartment), reverse micelles have been used [94]. In these complex fluids, small compartments of supersaturated aqueous solutions are stabilized within an oil using a surfactant (for example (2-ethylhexyl)sulfosuccinate, AOT) A precipitation is then induced inside each of these nanoreactors (either by chemical reaction of the precursors or by changing the temperature), which leads to the synthesis of nanoparticles whose size and shape is determined by the size and shape of the micelle. Anisotropic particles were grown by the addition of salts and/or co-surfactants that changed the micelle from spherical into roughly rod-like shapes [95]. A further development involved controlling the interfacial activity of the reverse micelles so that the nanoparticle synthesis and their self-assembly was coupled to give superlattices of shape controlled nanoparticles [96]. Face growth kinetics could even be used to tune the shape of the particles when the structure of the material targeted was highly anisotropic [97].

The third and most recent approach is an extension of the thoroughly studied carbon nanotube growth mechanism, namely the use of a growth promoter that helps in directing the growth of a material in a highly anisotropic manner [98]. The idea is to use a growth promoter nanoparticle (the diameter of which will drive the diameter of the nanowire) that can form a liquid alloy with the nanowire material of interest (Fig. 19). A careful study of the phase diagram allows the specific composition to be determined and the synthesis temperature necessary to achieve simultaneously the coexistence of the liquid alloy and the solid nanowire material. The liquid alloy nanoparticles act as preferred sites for the adsorption/dissolution of new reactant. When this alloy becomes supersaturated, it also acts as the nucleation site for recrystallization, leading to the growth of a nanowire.

### 6.1.2 Properties

However, apart from the examples developed above, the study of the self-assembly, in relation to the mesogenic properties for these suspensions of nanotubes,

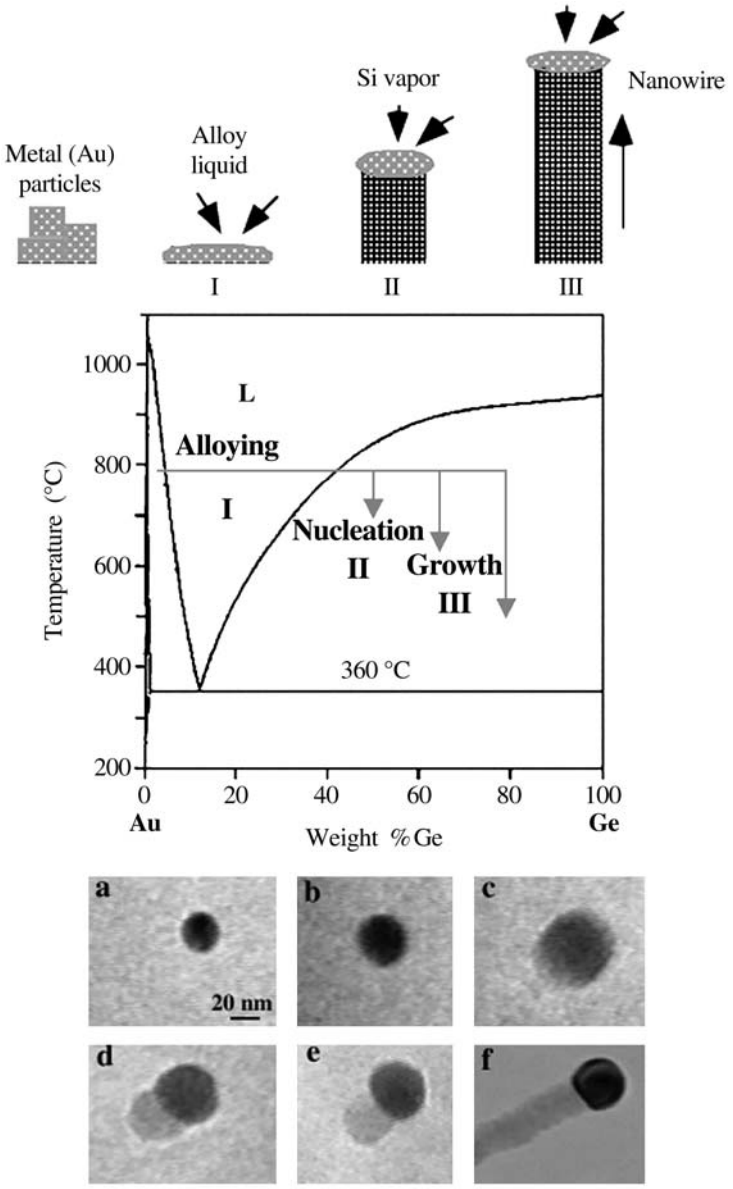


**Fig. 19.** Schematic illustration of vapor – liquid – solid nanowire growth mechanism including three stages: I) alloying, II) nucleation, and III) axial growth, as exemplified with the Au-Ge binary phase diagram (Au is a good solvent for the Ge nanowire growth because of the existence of the Au-Ge eutectic). This mechanism has been observed by in situ TEM that recorded images during the process of nanowire growth with: **a** Au nanoclusters in solid state at 500 °C; **b** alloying is initiated at 800 °C (Au now exists mostly in solid state); **c** liquid Au/Ge alloy; **d** nucleation of a Ge nanocrystal on the alloy surface; **e** Ge nanocrystal elongates with further Ge condensation; **f** eventually forms a wire. (Reprinted from [98b], copyright (2002) from John Wiley and Sons)

nanowires, and nanorods, is still in its infancy. A first challenge is to be able to reach a high enough concentration so as to obtain the Onsager nematic transition. We have seen that in the case of highly anisotropic charged particles, concentrations in the range of few percent by weight are usually necessary in order to observe such a transition. With much lower aspect ratio particles, such as nanorods or with uncharged moieties such as nanotubes, much higher concentrations are required. Also, many of these colloids are often too bulky and therefore do not form stable concentrated colloidal suspensions on their own. In most cases studied up to now, this problem has been overcome by stabilization of the suspension using either surfactants or by wrapping the colloids within a polymer therefore allowing highly concentrated suspensions to be obtained.

Another difficulty is that often only very small amounts of these anisotropic moieties can be synthesized at a time, limiting the study of the self-assembly properties to transmission electron microscopy analysis [135]. This makes it difficult to study in detail the phase diagram in concentration, usually a fairly sample consuming process. However, different approaches are currently being devised that give a taste of the huge potential that the self-assembly of these nanowires and nanorods can lead to.

A first way to circumvent the problem is to study the self-assembly of these anisotropic moieties within a 2-D Langmuir-Blodgett film. This was recently illustrated by P. Yang and co-workers using suspensions of $BaCrO_4$ nanorods synthesized by the reverse micelle approach [157]. Langmuir-Blodgett films obtained on the water surface and collected on a TEM grid display typical 2-D nematic and smectic organizations, and their topological defects. In Yang's report, a 2-D smectic to 3-D nematic transition is briefly mentioned that gives an insight into the bulk properties of such nanorods. However, as always in the case of TEM studies, it is difficult to determine exactly the role of drying. Note that in a related set of experiments, although the film was deposited by dip coating (directly from the bulk of the solution), the self-assembly properties of the carbon nanotubes bundles [99] allow the formation of fairly well oriented and therefore birefringent films of bundles. Such self-assembly of carbon nanotubes into a structure highly reminiscent of a nematic mesophase has been long awaited and discussed in meetings. Some alignment successes have even been reported when one combines nanotubes with some other liquid crystals, either lyotropic [100] or thermotropic [101]. Based upon our calculation using the Onsager model and our trials, in the case of bulk suspensions of neutral carbon nanotubes, we think that what has precluded the observation of a transition similar to what has been reported in the case of $Li_2Mo_6Se_6$ nanowire, imogolite or $NaNb_2PS_{10}$ nanotubes has been that the isotropic-nematic critical concentration is still higher than the highest concentration yet obtained. In the Zhou and co-workers' report, nanotube bundles have been shortened using a strong etching solution. The consequence is that the nanotubes are probably much more charged than the neutral pristine ones (due to the addition of carboxylic groups), which is known to decrease the critical transition concentration. We therefore expect for these suspensions that the pH of the solution should have a dramatic effect on the self-assembly properties reported.

Another method that has been developed for rapid screening of organic complex fluid phase diagrams consists of studying the drying of a suspension within

a capillary tube, directly on the beamline of a synchrotron. It is not an easy method for the quantitative determination of phase diagrams, but one may determine some phase transitions. Unfortunately, thermodynamic equilibrium is not usually reached and therefore this technique cannot be recommended.

Finally, a study of fairly monodisperse CdSe semiconducting nanorods functionalized with amphiphilic molecules in a suspension of cyclohexane has recently been published that shows preliminary results indicative of a typical nematic behavior [102]. Note that these nanorods have been synthesized by the pyrolysis of organometallic precursors of Cd and Se in hot surfactant mixture allowing a good control of the aspect ratio. This state of the art particle size and shape control method should allow one to customize accurately their semiconducting properties.

## 6.2 Use of MLC for the Structure Determination of Biomolecules by NMR

The first reported use of the mesogenic properties of MLC did not arise where one could have first expected it, i.e., liquid crystal displays, but in NMR. The classic NMR strategy for determining the conformation of a biomolecule [103] involves exploiting the combination of the scalar coupling, $^3J$, to obtain dihedral angle information and the $^1$H-$^1$H dipolar cross-relaxation rate, that has a $(1/r^6)$ dependence, where $r$ is the internuclear distance. The limitation of this approach is that only short-range structural information is obtained (a few bonds for the scalar coupling and distances inferior to 5 Å for the relaxation). As a consequence, if only few constraints per nucleus can be detected (e.g., multi-domain proteins, oligosaccharides, or oligonucleotides), the accumulation of errors can lead to an imprecise overall structure. In order to circumvent this problem, a different approach has recently been proposed using, in addition, structural data that are defined relative to an absolute molecular frame [104, 105]. Particularly interesting are methods that exploit residual dipolar couplings [105, 106]. However, as dipolar couplings are almost averaged to zero (tenths of Hz) because of the almost isotropic overall tumbling of the solute molecule, it is therefore necessary to make this tumbling motion more anisotropic. This can be achieved by replacement of the aqueous phase by an anisotropic medium such as a magnetically oriented mesophase [106]. As a consequence new couplings, $D$, add to the usual scalar couplings, $J$, to split the signals by a few Hz. By using pairs of spins separated by well known distances (any C-H or N-H bond) one can finally extract more precise and longer range structural information.

A few organic/biological liquid crystals (LC) have been used successfully for this purpose: surfactant-based bicelles, purple membranes, phages, and cellulose microcrystals [107]. We recently proposed using MLC to generate an anisotropic medium. Their inherent advantages are numerous: (i) some MLCs can be easily aligned when a magnetic field is applied, using only very small amounts of mineral materials (1–3 wt%, to be compared with 5–30% for bicelles, 10% for purple membranes, 5% for phages, and 8% for cellulose); (ii) these MLCs, which are sometimes formed using polar solvents other than water, present nematic phases that are stable on a very long time scale (few years) and over

a wide temperature range (the liquid state temperature range of the solvent), in stark contrast with the organic LC systems whose stability is often an experimental problem for this type of NMR method [108]; (iii) the dissolved biomolecule can simply be recovered after the experiment by flocculation of the mineral colloid; (iv) finally, the absence of $^{1}H$ and $^{13}C$ nuclei renders isotope labeling of the studied molecule unnecessary, whereas, in the case of organic liquid crystals, the NMR signal is strongly dominated by the liquid crystal resonances due to the high ratio of LC molecules to biomolecules. This is obviously a major advantage especially for systems such as oligosaccharides or oligonucleotides for which labeling is chemically challenging and particularly expensive.

We therefore demonstrated the potential of such MLC for NMR structural characterization by reporting residual C-H dipolar couplings observed for nonlabeled saccharide containing the Lewis$^{X}$ motif of various flexibility dissolved in aqueous suspension of $V_2O_5$ [109], as well as $H_3Sb_3P_3O_{14}$ [61, 110, 111].

### 6.3
### Use of Flow Alignment and Pretransitional Effect Toward Applications

We have seen that it can be difficult to reach the critical concentration required to observe an isotropic-anisotropic transition because concentrated suspensions of colloids are not always stable. However, orientation of flexible polymers as well as of anisotropic particles in suspension can be induced by flow, a phenomenon that has long been observed, reported, and studied. This phenomenon is especially strong when a pretransitional effect exists, which can be easily observed by the naked eye on a sample that is shaken between crossed polarizers (see for example the section on clays). In these systems, birefringence is induced via mechanical forces, like the shear stresses in a laminar flow ("Maxwell-dynamo-optic effect").

One can therefore take advantage of this alignment effect when anisotropic materials are desired. In a first example, the mesomorphic properties of $Li_2Mo_6Se_6$ that we had previously demonstrated were used to synthesize: (i) highly oriented conducting thin films by spin coating the pure material (after solvent evaporation); (ii) oriented composites by extrusion [112].

Another example comes from the fact that up to recently one could not store beer in plastic bottles because gas diffusion (in and out) through the bottle walls was too large. Composites have now been developed by dispersing clay particles within a polymer. The particles are aligned by flow during extrusion, parallel to the bottle walls. Because of this orientation, the clay particles can play a barrier role and drastically reduce gas diffusion. The charge of the clay also allowed improvements of the mechanical properties of these composites materials [113]. Highly oriented extruded polymer-carbon nanotube composites have been obtained using flow orientation [114] that show very anisotropic properties, including electrical conductivity (with high conductivity only along the axis of extrusion). Such anisotropic conductivity can be useful for some applications but not for the conducting composites used in the new generation of reversible fuses that are widely employed nowadays by the semiconducting and electronic industry [115].

More recently, the flow alignment of suspensions of nanowires has been combined with microfluidic technology [116]. In this development, suspensions of nanowires/nanotubes are flowed within microchannels formed in a PDMS mold and deposited on a silicon wafer substrate (Fig. 20a,b). This allows parallel arrays of NW aligned along the flow direction when the mold is removed to be obtained. Multiply crossed NW arrays can then be built by changing the flow direction sequentially by iterating this process using a succession of molds with channels oriented along different axes (Fig. 20b).

### 6.4 Composites Materials

We have seen that only in a few cases have some composites materials based on MLC been made. Out of those only in the case of $Li_2Mo_6Se_6$ was the mesogenic

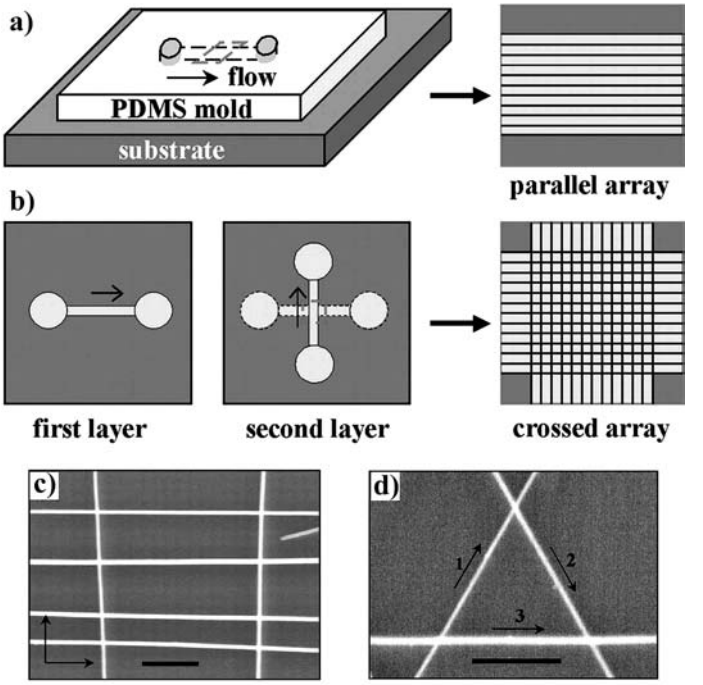


**Fig. 20a–d.** Schematic of fluidic channel structures for flow assembly and layer-by-layer assembly of crossed NW arrays: **a** NW assembly is carried out by controlling the flow of a NW suspension inside the channel (made from the mold-substrate assembly) – arrays of NWs are oriented parallel to the flow direction on the substrate ( after removal of PDMS mold); **b** multiple crossed NW arrays are created by changing the flow direction sequentially in a layer-by-layer assembly process – typical SEM image of crossed arrays of NWs obtained in an assembly process (flow directions are highlighted by *arrows* in the images) comprising: **c** two sequential steps with orthogonal flow directions (InP NWs); **d** three sequential steps with 60° angles between flow directions (GaP NWs). The *scale bars* correspond to 500 nm in c and d. (Reprinted from [116], copyright 2001 American Association for the Advancement of Science)

property purposely used to organize the final material. We develop below two other recent examples.

### 6.4.1
### *Mesoporous Materials Based on MLC Templates*

We recently showed that it is possible to synthesize a mesoporous composite material by direct assembly of anisotropic hollow objects [117]. In this study we used stable colloidal suspensions of well defined tubular structure made from the scrolling of the sheets themselves obtained by the exfoliation of the acid-exchange $K_4Nb_6O_{17}$ with tetra-(*n*-butyl)-ammonium hydroxide in water [118]. Detailed physicochemical studies of these colloidal suspensions at high concentration are still in progress [119]; however we thought they would be good candidates to make a silicate-nanotubule composite. The synthesis of our composite material (CMI-1) was adapted from the procedure of Goltsov et al. [120], but now using the organized nanotubules instead of an organic surfactant. Nitrogen physisorption experiments performed on this composite exhibited type IV behavior (hysteresis), typical of materials with large pores with restricted openings (ink bottle). This material has an $N_2$ Brunauer-Emmett-Teller (BET) surface area of 102 $m^2/g$, a mean pore size of 14.6 nm, and a single point (p/p0=0.965) pore volume of 0.32 $cm^3/g$. This mean pore size is in agreement with the mean inner diameter determined by TEM (15.5 Å). This use of mineral liquid crystals represents a new approach for the synthesis of composite porous materials and thus diversifies the types of objects that can be assembled in this way, offering the possibility of synthesizing new materials with a variety of properties.

This work has been further developed using $V_2O_5$ nanoribbons instead of the $[Nb_6O_{17}^{4-}]_n$ nanotubules [121]. The use of a magnetic field during the condensation of the silicate framework allowed us to obtained centimeter sized single-domain monoliths in which the nematic mineral liquid crystals are well aligned. Total removal of the MLC can also easily be achieved leaving transparent mesoporous birefringent silica with complete retention of the magnetically aligned channels director, even for centimeter sized samples.

### 6.4.2
### *Hybrid Organic-Inorganic Solar Cells*

In a recent publication, Alivisatos and co-workers reported the making of hybrid nanorods-polymer solar cells and their properties [122]. These solar cells were made by spin casting of a solution of both poly(3-hexylthiophene) (hole acceptor) and CdSe nanorods (electron acceptor) onto indium tin oxide glass substrates coated with poly(ethylene dioxythiophene) doped with polystyrene sulfonic acid and aluminum as a top contact. Nanorods have been used in composites so as to improve the carrier mobility. Indeed, the latter can be high for some inorganic semiconductors, but it is typically extremely low for conjugated polymers [123]. The use of the nanorods supplies an interface for the charge transfer as well as a direct path for electrical transport. Also, because of their anisotropy, self-assembly of these nanorods is observed by electron microscopy. It shows

that the nanorods are partially aligned perpendicular to the substrate plane. The orientation of the nanorods as a function of their aspect ratio is predicted to play a crucial role in the properties of these new devices, as it should have a strong impact on the formation of percolation pathways for electron transport.

## 6.5 Hybrid Bio-Mineral Mesogens

A superb liquid crystal system was recently created by Belcher and co-workers that allowed them to produced a highly ordered composite material from genetically engineered M13 bacteriophage and zinc sulfide (ZnS) nanocrystals [124]. The mesogenic properties of the bacteriophage [125], which was selected for its specific recognition for ZnS crystal surfaces [126] (Fig. 21), were used to trigger the self-assembly. Indeed, bacteriophages were coupled with ZnS solution precursors and spontaneously evolved into a self-supporting hybrid film material that was ordered both at the nanoscale and at the micrometer scale and which was continuous over a centimeter length scale.

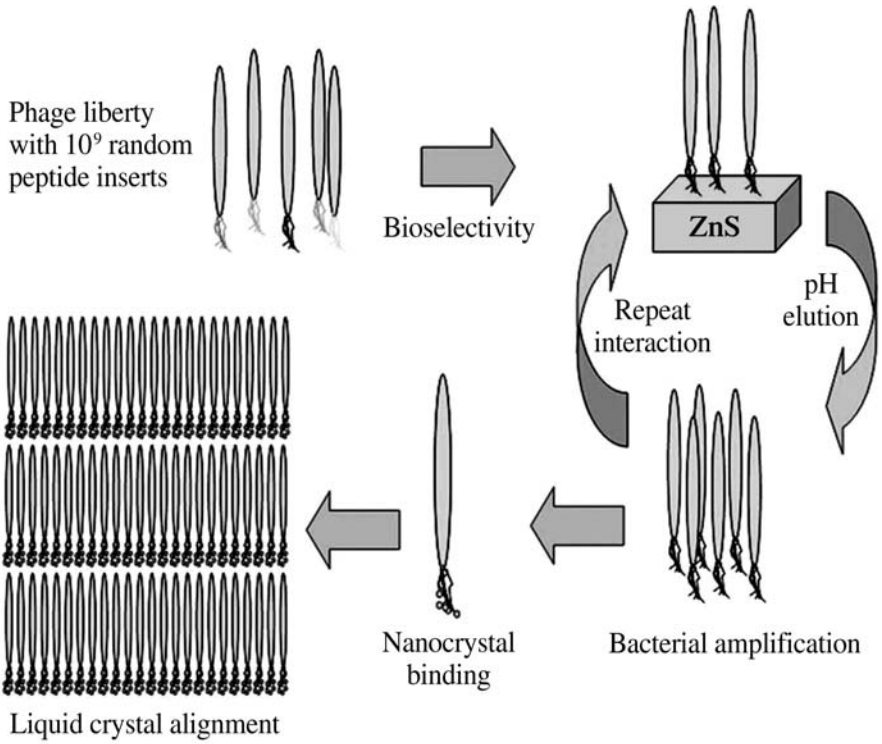


**Fig. 21.** Schematic diagram of the process used to generate nanocrystal alignment by the phage display method. (Reprinted with permission from [124], copyright 2000, American Association for the Advancement of Science)

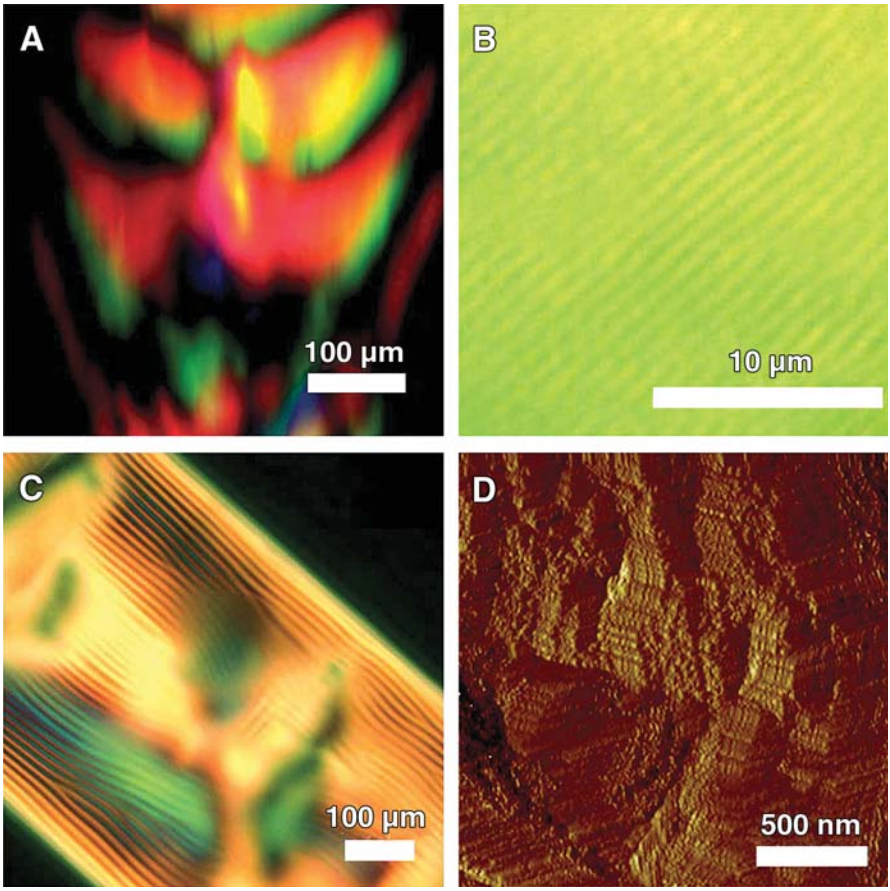


**Fig. 22A–D.** Characterization of the liquid crystalline suspensions of A7 phage-ZnS nanocrystals (A7-ZnS) and cast film: **A** POM texture of a suspension of A7-ZnS (127 mg/ml); **B, C** their constructive and destructive interference patterns generated from parallel aligned smectic layers when observed using a differential interference contrast filter; **D** texture of the cholesteric phase of an A7-ZnS suspension (76 mg/ml). (Reprinted with permission from [124], copyright 2000, American Association for the Advancement of Science)

In addition, the liquid crystalline phase behavior of these suspensions could be controlled by solvent concentration as well as by the use of a magnetic field. These suspensions and films observed by optical microscopy showed textures indicative of the smectic and cholesteric structure of the hybrid systems (Fig. 22).

## 7 Perspectives

Let us here briefly discuss a few guidelines useful for the search of new mineral liquid crystalline suspensions. This discussion tries to summarize the subtle balance between excluded volume interactions, electrostatic repulsions, and Van der Waals attractions that is needed to stabilize the nematic phase with respect to the isotropic one and flocculation or recrystallization.

An obvious criterion is that the mineral moieties of interest have to be able to be dispersed in a suitable solvent in large enough concentrations. We have seen several examples of how this can be achieved by exfoliation or by direct self-assembly from molecular precursors. This dispersion step is probably one of the most delicate points to fulfill.

Another related criterion is that the colloidal moieties should be as anisotropic as possible. This can be quantitatively predicted in the frame of the Onsager model. The volume fraction at which nematic ordering occurs is $\Phi \approx 4D/L$, which is 40% in the case of rods of aspect ratio 10 interacting through a purely hard-core potential. This is still quite a large volume fraction. In contrast, rods of aspect ratio 100 will order at a much more reasonable value of 4%. Moreover, both theory and numerical simulations show that particles of aspect ratio smaller than 3–4 never order in a nematic phase whatever their volume fraction. These orders of magnitude illustrate the need for fairly anisotropic moieties.

A parameter that cannot be over looked is the dispersity in size of the particles. Indeed, polydispersity usually prevents long range positional ordering. For example, it is crucial in order to obtain (i) smectic phases to have nanoparticles of fairly homogeneous length and (ii) hexagonal phases to have nanoparticles with diameters as monodisperse as possible.

The charge of the building blocks within mineral liquid crystalline suspensions should also be considered in detail since electrostatic repulsions play two important roles. First, these interactions often ensure colloidal stability against Van der Waals attractions. Second, the existence of clouds of counter-ions increase the effective volume fraction of anisotropic moieties in suspension, which helps to attain the phase transition threshold. Moreover, there is a large entropy gain associated with the release of the counter-ions in solution, which stabilizes the nematic suspension. Therefore, charged moieties are better candidates. However, in the case of neutral moieties, grafting with a polymer layer seems to be an efficient way of preventing particle aggregation.

Flexibility of the moieties is another important parameter because it was recently shown that flexible objects require larger volume fractions to undergo nematic ordering. Flexibility also reduces the nematic order parameter at the transition. Intuitively, very flexible mineral polymers should not show any orientational order at rest, but may display a strong flow birefringence. Thus, any soluble system where the structural unit in the solid state is anisotropic may not necessarily be a lyotropic liquid crystal. For example, in solution a polymer is much less constrained than in the solid state, and hence one must consider the elastic properties of the polymer chain and whether the anisotropic units still exist in solution. As shown recently for the case of the complex fluid with a min-

eral core based upon the 1-D polyelectrolyte $^{1}_{\infty}[MPS_4]^-$ (M=Ni, Pd) dissolved in DMF [6], the polymer chain is highly flexible and may even, depending upon the metal M and the temperature, fragment and lose its complex fluid properties. High flexibility does not however preclude self-assembly when folding of the polymer leading to unexpected superstructures [34].

We have only described here the mineral mesophases that have been fully and unambiguously characterized. This review article is therefore not exhaustive. Other less well-documented examples can be found in the literature, in particular in another review article [127, 128]. Nevertheless, the diversity of examples described here should draw the attention of the reader to the fact that suspensions based on anisotropic structural units may be liquid crystalline, a feature that could be used to obtain a better understanding/optimization of materials synthesis and processing conditions. Thus, the existence of a nematic domain in the phase diagram together with the possibility of growing reproducibly oriented single domains on the centimeter scale could be used, for instance, in the field of pillared materials to produce better structured materials.

The main interest of mesophases based on mineral moieties is, in contrast to their organic counterparts, that they can be electron rich and so have enhanced electrical, optical, and magnetic properties. In addition, mineral moieties are thermally very stable. Thus, combined with their typically very wide range of temperature stability of mesomorphic organization, it can be envisaged that they can be used for applications under extreme conditions. Another important and common asset of these MLC is their very low cost since some of them can even be found in a natural form. This will allow their use for massive material production.

Finally, since MLC are based on anisotropic nanosystems, the understanding of their collective properties, either pre- or post-transitional, is of prime importance to allow their manipulation and therefore for the development of applications in the field of nanotechnology.

**Acknowledgements.** We are deeply indebted to many colleagues for instructive discussions and to our coworkers whose listing would be too long. However, we particularly wish to express our gratitude to Patrick Batail and Jacques Livage who have persistently supported us in this new avenue of research, to our PhD students, Olivier Pelletier, Franck Camerel, and Bruno Lemaire as well as to H.N.W. Lekkerkerker and L.M. Bull for their critical review of the manuscript. Finally, we would like to thank Wiley-VCH Verlag GmbH & Co. who kindly granted us permission to use in this article parts of our previous review article [4b], copyright 2000

## References

1. De Gennes PG, Prost J (1995) The physics of liquid crystals. Clarendon Press, Oxford
2. Tschierske C (1998) J Mater Chem 8:1485
3. Demus D, Goodby JW, Gray GW, Spiess HW, Vill V (eds) (1998) Handbook of liquid crystals. Wiley, Weinheim
4. a) Davidson P, Batail P, Gabriel JCP, Livage J, Sanchez C, Bourgaux C (1997) Prog Polym Sc 22:913; b) Gabriel JCP, Davidson P (2000) Adv Mater 12:9
5. Gabriel JCP, Uriel S, Boubekeur K, Batail P (2001) Chem Rev 101:2037

6. Sayettat J, Bull LM, Gabriel JCP, Jobic S, Camerel F, Marie AM, Fourmigué M, Batail P, Brec R, Inglebert RL (1998) Angew Chem Int Ed 37:1711
7. Oriol L, Serrano JL (1995) Adv Mater 7:348
8. Zocher H (1925) Z Anorg Allg Chem 147:91
9. Langmuir I (1938) J Chem Phys 6:873
10. Onsager L (1949) Ann NY Acad Sci 51:627
11. See, for instance, Samborski A, Evans GT, Mason CP, Allen MP (1994) Mol Phys 81:263
12. Guinier A, Fournet G (1955) Small angle scattering of X-rays. Wiley, New York
13. Synthesis of $M_2Mo_6Se_6$: a) M=Tl. In: Potel M, Chevrel R, Sergent M (1980) Acta Cryst B 36:1545; b) (M=Li, Na, K, Rb, Cs) Tarascon JM, Hull GW, DiSalvo FJ (1984) Mater Res Bull 19:915
14. Most members of the family, $M_2Mo_6Y_6$ (M=Na, In, K, Rb, Cs, Tl, Y=chalcogen), are pseudo-one-dimensional metals with even a superconductor at 3 K with $Tl_2Mo_6Se_6$: a) Armici JC, Decroux M, Fisher Ø, Potel M, Chevrel R, Sergent M (1980) Solid State Comm 33:607; b) Potel M, Chevrel R, Sergent M, Armici JC, Decroux M, Fisher Ø (1980) J Solid State Chem 35:286
15. Tarascon JM, DiSalvo FJ, Chen CH, Carrol PJ, Walsh M, Rupp L (1985) J Solid State Chem 58:290
16. Gabriel JCP (1993) PhD Thesis, University Paris XI, Orsay
17. a) Davidson P, Gabriel JC, Levelut AM, Batail P (1993) Europhys Lett 21:317; b) Davidson P, Gabriel JC, Levelut AM, Batail P (1993) Adv Mater 5:665
18. Fuhrer MS, Nygard J, Shih L, Forero M, Yoon Y, Mazzoni MSC, Choi H, Ihm J, Louie SG, Zettl A, McEuen PL (2000) Science 288:494
19. Messer B, Song JH, Huang M, Wu YY, Kim F, Yang PD (2000) Adv Mater 12:1526
20. Song JH, Messer B, Wu YY, Kind H, Yang PD (2001) J Am Chem Soc 123:9714–9715
21. Venkataraman L, Lieber CM (1999) Phys Rev Lett 83:5334
22. Bronger W, Müller P (1984) J Less Comm Met 100:241
23. Lu YJ, Ibers JA (1993) Comments Inorg Chem 14:229
24. For example, this was observed in the case of the series $Na_{2-x}Li_xMo_6Se_6$ (x=0–2) [15]
25. a) Farmer C, Fraser AR, Tait JM (1977) Chem Comm 462; b) Wada S-I, Eto A, Wada K (1979) J Soil Sci 30:347; c) Wada S-I (1987) Clays Clay Miner 35:379
26. Barett SM, Budd PM, Price C (1991) Eur Polym J 27:609; d) US Pats 4,252,779 and 4,241,035
27. Koenderink GH, Kluijtmans SGJM, Philise AP (1999) J Colloid Interface Sci 216:429
28. In the case of synthetic Imogolite, it seems that the diameter of the cylinder is 28 Å, slightly more that the natural one
29. a) Kajiwara K, Donkai N, Hiragi Y, Inagaki H (1986) Makromol Chem 187:2883; b) Kajiwara K, Donkai N, Fujiyoshi Y, Inagaki H (1986) Makromol Chem 187:2895; c) Donkai N, Kajiwara K, Schmidt M, Miyamoto T (1993) Makromol Chem Rapid Comm 14:611
30. Donkai N, Hoshino H, Kajiwara K, Miyamoto T (1993) Makromol Chem 194:559
31. a) Livolant F, Leforestier A (1996) Prog Polym Sc 21:1115; b) Giraud-Guille MM (1998) Curr Opin Solid State Mater Sci 3:221
32. a) Hoshino H, Yamana M, Donkai N, Sinigerski V, Kajiwara K, Miyamoto T, Inagaki H (1992) Polym Bull 28:607; b) Hoshino H, Ito T, Donkai N, Urakawa H, Kajiwara K (1992) Polym Bull 29:453
33. Ramos L, Molino F, Porte G (2000) Langmuir 16:5846
34. Camerel F, Gabriel JCP, Davidson P, Schmutz M, Gulik-Krzywicki T, Lemaire B, Bourgaux C, Batail P (2002) Nanoletters 2:403
35. Livage J (1991) Chem Mater 3:578
36. Bailey JK, Nagase T, Pozarnsky GA, MeCartney ML (1990) Mat Res Soc Symp Proc 180:759; b) Pozarnsky GA, McCormick AV (1994) Chem Mater 6:380; c) Livage J (1998) Coord Chem Rev 178/180:999; d) Pelletier O, Davidson P, Bourgaux C, Coulon C, Regnault S, Livage J (2000) Langmuir 16:5295

37. a) Davidson P, Garreau A, Livage J (1994) Liq Cryst 16:905; b) Davidson P, Bourgaux C, Schoutteten L, Sergot P, Williams C, Livage J (1995) Phys II (France) 5:1577; c) Pelletier O, Bourgaux C, Diat O, Davidson P, Livage J (2000) Eur Phys J E 2:191
38. Pelletier O, Bourgaux C, Diat O, Davidson P, Livage J (1999) Eur Phys J B 12:541
39. Commeinhes X, Davidson P, Bourgaux C, Livage J (1997) Adv Mater 9:900
40. Panar M, Beste LF (1977) Macromolecules 10:1401; b) Sridhar CG, Hines WA, Samulski ET (1974) J Chem Phys 61:947
41. Srajer G, Fraden S, Meyer RB (1989) Phys Rev A 39:4828
42. Davidson P, Petermann D, Levelut AM (1995) J Phys II (France) 5:113
43. Pelletier O, Davidson P, Bourgaux C, Livage J (1999) Europhys Lett 48:53
44. Pelletier O, Sotta P, Davidson P (1999) J Phys Chem B 103:5427
45. Lamarque-Forget S, Pelletier O, Dozov I, Davidson P, Martinot-Lagarde P, Livage J (2000) Adv Mater 12:1267
46. Van Olphen H (1977) An introduction to clay colloid chemistry. Wiley, New York
47. a) Burger J, Sourieau P, Combarnous M (1985) Thermal methods of oil recovery. Technip, Paris; b) Pinnavaia TJ (1983) Nature 220:365; c) Kojima Y, Usuki A, Kawasumi M, Okada A, Kurauchi T, Kagimaito O, Kaji K (1995) J Polym Sci B 33:1039
48. EmersonWW (1956) Nature 178:1248
49. a) Mourchid A, Delville A, Lambard J, Lécolier E, Levitz P, (1995) Langmuir 11:1942; b) Mourchid A, Lécolier E, Van Damme H, Levitz P (1998) Langmuir 14:4718; Pignon F, Piau JM, Magnin A (1996) Phys Rev Lett 76:4857; c) Pignon F, Magnin A, Piau JM (1997) Phys Rev Lett 79:4689; d) Pignon F, Magnin A, Piau JM, Cabane B, Lindner P, Diat O (1997) Phys Rev E 56:3281; e) Bonn D, Tanaka H, Wegdam G, Kellay H, Meunier J (1998) Europhys Lett 45:52; f) Bonn D, Kellay H, Tanaka H, Wegdam G, Meunier J (1999) Langmuir 15:7534
50. Gabriel JCP, Sanchez C, Davidson P (1996) J Phys Chem 100:11,139
51. a) Forsyth PA, Marcelja JS, Mitchell DJ, Ninham BW (1978) Adv Colloid Interface Sci 9:37; b) Eppenga R, Frenkel D (1984) Mol Phys 52:1303; c) Frenkel D (1989) Liq Cryst 5:929
52. Lemaire BJ, Panine P, Gabriel J-CP, Davidson P (2002) Europhys Lett (in press)
53. Morvan M, Espinat D, Lambard J, Zemb T (1994) Colloid Surf A 82:193
54. Forsyth PA, Marcelja JS, Mitchell DJ, Ninham BW (1978) Adv Colloid Interface Sci 9:37
55. Mourchid A, Levitz P (1998) Phys Rev E 57:R4887 and references cited therein
56. Levitz P, Lécolier E, Mourchid A, Delville A, Lyonnard S (2000) Europhys Lett 49:672
57. a) Saunders JM, Goodwin JW, Richardson RM, Vincent B (1999) J Phys Chem B, 103:9211; b) Ramsay JDF, Lindner P (1993) J Chem Soc Faraday Trans, 89:4207; c) Ramsay JDF, Swanton SW, Bunce J (1990) J Chem Soc Faraday Trans 86:3919; d) DiMasi E, Fossum JO, Gog T, Venkataraman C (2001) Phys Rev E, 64:061704; e) Porion P, Al Mukhtar M, Faugère AM, van der Maarel JRC, Delville A (2001) J Phys Chem B 105:10505
58. Bihannic I, Michot LJ, Lartiges BS, Vantelon D, Labille J, Thomas F, Susini J, Salomé M, Fyard B (2001) Langmuir 17:4144
59. Cousin F, Cabuil V, Levitz P (2002) Langmuir 18:1466
60. A new study of the salt-induced ordering in lamellar colloids appeared while this paper was in press: Rowan DG, Hansen JP (2002) Langmuir 18:2063–2068
61. Gabriel JCP, Camerel F, Lemaire BJ, Desvaux H, Davidson P, Batail P (2001) Nature 413:504
62. Piffard Y, Verbaere A, Lachgard A, Deniard-Courant S, Tournoux M (1986) Rev Chim Gen 23:766
63. Zocher H, Torök C (1960) Kolloid Zeit170:140; b) Zocher H, Torök C (1960) Kolloid Zeit 173:1; c) Zocher H, Torök C (1962) Kolloid Zeit 180:41
64. Bugosh J (1961) J Phys Chem 65:1789
65. a) Buining PA, Pathmamanoharan C, Jansen JBH, Lekkerkerker HNW (1991) J Ceram Soc 74:1303; b) Buining PA, Philipse AP, Lekkerkerker HNW (1994) Langmuir 10:2106; c) van Bruggen MPB, Donker M, Lekkerkerker HNW, Hugues TL (1999) Colloid Surf 150:115; d) Buining PA, Veldhuizen YSJ, Pathmamanoharan C, Lekkerkerker HNW (1992) Colloid Surf 64:47; e) Buining PA, Lekkerkerker HNW (1993) J Phys Chem 97:11,510; f) Vroege GJ, Lekkerkerker HNW (1993) J Phys Chem 97:3601
66. van Bruggen MPB, Dhont JKG, Lekkerkerker HNW (1999) Macromolecules 32:2256

67. a) Deryagin BV, Landau L (1941) Acta Physicochim URSS 333:55; b) Verwey E, Overbeek JW (1948) Theory of the stability of lyophobic colloids. Elsevier, Amsterdam
68. Israelachvili JN (1991) Intermolecular and surface forces. Academic Press, London
69. Pelletier O, Davidson P, Bourgaux C, Livage J (1999) Progr Colloid Polym Sci 112:121
70. a) van Bruggen MPB, Lekkerkerker HNW, Dhont JKG (1997) Phys Rev E 56:4394; b) Wierenga AM, Philipse AP, Reitsma EM (1997) Langmuir 13:947; c) Wierenga AM, Philipse AP, Lekkerkerker HNW, Boger DV (1998) Langmuir 14:55; d) van Bruggen MPB, Lekkerkerker HNW, Maret G, Dhont JKG (1998) Phys Rev E 58:7668
71. Van der Kooij F, Lekkerkerker HNW (1998) J Phys Chem B 102:7829
72. Bates MA, Frenkel D (1999) J Chem Phys 110:6553
73. Chandrasekhar S, Sadashiva BK, Suresh KA (1977) Pramana 7:471
74. Brown ABD, Clarke SM, Rennie AR (1998) Langmuir 14:3129
75. Brown ABD, Ferrero C, Narayanan T, Rennie AR (1999) Eur Phys J B 11:481
76. Veerman JAC, Frenkel D (1992) Phys Rev A 45:5632
77. Brown ABD, Rennie AR (2000) Phys Rev E 62:851
78. van der Kooij FM, Kassapidou K, Lekkerkerker HNW (2000) Nature 406:868
79. van der Kooij FM, van der Beek D, Lekkerkerker HNW (2001) J Phys Chem B 105:1696
80. Wensink HH, Vroege GJ, Lekkerkerker HNW (2001) J Phys Chem B 105:10,610
81. van der Kooij FM, Lekkerkerker HNW (2000) Phys Rev Lett 84:781
82. Wensink HH, Vroege GJ, Lekkerkerker HNW (2001) J Chem Phys 115:7319
83. van der Kooij FM, Lekkerkerker HNW (2000) Langmuir 16:10,144
84. Zocher H, Jacobsohn K (1929) Kolloid Beih 28:167
85. Heller W (1935) Compt Rend 201:831; b) Heller W (1980) Polymer colloids II. Fitch E (ed) Plenum Press, New York, and references cited therein
86. a) Maeda Y, Hachisu S (1983) Colloids Surf 6:1; b) Maeda H, Maeda Y (1996) Langmuir 12:1446
87. Cornell RM, Schwertmann U (1996) The iron oxides. VCH, Weinheim
88. Lemaire BJ, Davidson P, Ferre J, Jamet JP, Panine P, Dozov I, Jolivet JP (2002) Phys Rev Lett 88:125,507
89. Iijima (1991) Nature 354:56
90. a) Ozin GA (1992) Adv Mater 4:612; b) Martin CR (1994) Science 266:1961; c) Martin CR (1996) Acc Chem Res 28:61
91. Wu CG, Bein T (1994) Science 266:1013
92. a) Piraux L, George JM, Despres JF, Leroy C, Ferain E, Legras R, Ounadjela K, Fert A (1994) Appl Phys Lett 65:2484; b) Fert A, Piraux L (1999) J Magn Magn Mater 200:338
93. a) Martin BR, Dermody DJ, Reiss BD, Fang MM, Lyon LA, Natan MJ, Mallouk TE (1999) Adv Mater 11:1021; b) Nicewarner-Pena SR, Freeman RG, Reiss BD, He L, Pena DJ, Walton ID, Cromer R, Keating CD, Natan MJ (2001) Science 294:137
94. Lisiedki I, Pileni MP (1993) JACS 115:3887
95. a) Tanori J, Pileni MP (1995) Adv Mater 7:862; b) Tanori J, Pileni MP (1997) Langmuir 13:639; c) Filankenbo, Pileni MP (2000) Appl Surf Science 164:260
96. Li M, Schnablegger H, Mann S (1999) Nature 402:393
97. Peng X, Manna L, Yang W, Wickham J, Scher E, Kadavanich A, Alivisatos AP (2000) Nature 404:59
98. a) Hu J, Odom TW, Lieber CM (1999) Acc Chem Res 32:435; b) Wu Y, Yan H, Huang M, Messer B, Song JH, Yang P (2002) Chem Eur J 8:1261
99. Shimoda H, Oh SJ, Geng HZ, Walker RJ, Zhang XB, McNeil LE, Zhou O (2002) Adv Mater 14:899
100. Vigolo B, Penicaud A, Coulon C, Sauder C, Pailler R, Journet C, Bernier P, Poulin P (2000) Science 290:1331
101. Lynch MD, Patrick DL (2002) Nanoletters (in press)
102. Li LS, Walda J, Manna L, Alivisatos AP (2002) Nano Lett 2:557
103. Wüthrich K (1986) NMR of proteins and nucleic acids. Wiley Interscience, New York
104. Tjandra N, Garrett DS, Gronenborn AM, Bax A, Clore GM (1997) Nat Struct Biol 4:443

105. Tjandra N, Omichinski JG, Gronenborn AM, Clore GM, Bax A (1997) Nat Struct Biol 4:732
106. Tjandra N, Bax A (1997) Science 278:1111
107. For a quick review: Prestegard JH, Kishore AI (2001) Curr Opin Chem Biol 5:584 and references therein
108. Losonczi JA, Prestegard JH (1998) J Biomol NMR 12:47
109. Desvaux H, Gabriel JCP, Berthault P, Camerel F (2001) Angew Chem Int Ed 40:373
110. Berthault P, Jeannerat D, Zhang Y, Camerel F, Alvarez-Salgado F, Boulard Y, Sinaÿ P, Gabriel JCP, Desvaux H (submitted)
111. See www graphical abstract that represent biomolecules within $H_3Sb_3P_3O_{14}$ sheets
112. a) Golden JH, DiSalvo FJ, Fréchet JMJ (1995) Chem Mater 7:232; b) Golden JH, DiSalvo FJ, Fréchet JMJ, Silcox J, Thomas M, Ellman J (1996) Science 273:782
113. Here are few examples of patents of composites based on a dispersed clay with enhanced mechanical or gas barrier properties: US4472538, US4739007, US4889885, US4894411, EP0352042, EP0398551, WO9304117, WO9304118, WO9311190, US5385776, US5514734, EP0358415
114. Vigolo B, Penicaud A, Coulon C, Sauder C, Pailler R, Journet C, Bernier P, Poulin P (2000) Science 290:1331
115. Chang J. Personnal communication
116. Huang Y, Duan X, Wei Q, Lieber CM (2001) Science 291:630
117. Camerel F, Gabriel JCP, Batail P (2002) Chem Comm 1926
118. Saupe GB, Waraksa CC, Kim HN, Han YJ, Kaschak DM, Skinner DM, Mallouk TE (2000) Chem Mater 12:1556
119. A nice optical study of this MLC ($K_4Nb_6O_{17}$ sols) appeared while this paper was in Press: Miyamoto N, Nakato T (2002) Adv Mater 14:1267
120. Goltsov YG, Matkovskaya LA, Smelaya ZV, Il'in VG (1999) Mendeleev Commun 241
121. a) Camerel F (2001) PhD Thesis, Nantes University, France; b) Camerel F, Gabriel JCP, Batail P (2002) In Press, Adv Funct Mater
122. Huynh WU, Dimer JJ, Alivisatos AP (2002) Science 295:2425
123. Borazano L, Carte SA, Scott JC, Malliaras GG, Brock PJ (1999) Appl Phys Lett 74:1132
124. Lee SW, Mao C, Flynn CE, Belcher AM (2002) Science 296:892
125. a) Dogic Z, Fraden S (1997) Phys Rev Lett 78:2417; b) Dogic Z, Fraden S (2000) Langmuir 16:7820; c) Lapointe J, Marvin DA (1973) Mol Cryst Liq Cryst 19:269; d) Issaenko A, Harris SA, Lubensky TC (1999) Phys Rev E 60:578
126. It has been shown recently that engineered viruses can recognize specific semiconductor surfaces using the method of selection by combinatorial phage display: Whaley R, English DS, Hu EL, Barbara PF, Belcher AM (2000) Nature 405:665
127. Sonin AS (1998) Colloid J 60:129
128. A report of a possible new MLC appeared while this manuscript was in press: Backov R, Morgan AN, Lane S, Perez-Cordero EE, Williams K, Meisel MW, Sanchez C, Talham DR (2002) Mol Cryst Liq Cryst 376:127
129. A review of oxidic nanotubes and nanorods has been published while this manuscript was in press: Patzke GR, Krumeich F, Nesper R (2002) Angew Chem Int Ed 41:2446
130. Here are few examples of reviews on the subject: a) Sinnott SB, Andrews R (2001) Crit Rev Solid State Mater Sciences 26:145; b) Rao CNR, Satishkumar BC, Govindaraj A, Nath M (2001) Chem Phys Chem 2:78; c) Rakov EG (2000) Uspekhi Khimii 69:41; d) Ajayan PM (1999) Chem Rev 99:1787
131. a) Zhang QM, Li Y, Xu DS, Gu ZN (2001) J Mater Sci Lett 20:925; b) Zhu JJ, Liao XH, Zhao XN, Chen HY (2001) Mater Lett 49:91; c) Lin SW, Yue J, Gedanken A (2001) Adv Mater 13:656; d) Jana NR, Gearheart L, Murphy CJ (2001) Chem Comm 2001:617; e) Bhattacharyya S, Saha SK, Chakravorty D (2000) Appl Phys Lett 77:3770; f) Kyoung M, Lee M (1999) Opt Commun 171:145; g) Link S, El-Sayed MA (1999) J Phys Chem B 103:8410; h) Sloan J, Wright DM, Woo HG, Bailey S, Brown G, York APE, Coleman KS, Hutchison JL, Green MLH (1999) Chem Comm 1999:699; i) Zhou Y, Yu SH, Cui XP, Wang CY, Chen ZY (1999) Chem Mater 11:545; j) Korgel BA, Fitzmaurice D (1998) Self-assembly of

silver nanocrystals into two-dimensional nanowire arrays. Adv Mat 10:661; k) Han YJ, Kim JM, Stucky GD (2000) Chem Mater 12:2068
132. a) Jana NR, Gearheart L, Murphy CJ (2001) J Phys Chem B 105:4065; b) Mbindyo JKN, Reiss BD, Martin BR, Keating CD, Natan MJ, Mallouk TE (2001) Adv Mat 13:249; c) Wang BL, Yin SY, Wang GH, Buldum A, Zhao JJ (2001) Phys Rev Lett 86:2046; d) Ramsperger U, Uchihashi T, Nejoh H (2001) Appl Phys Lett 78:85; e) Yu JS, Kim JY, Lee S, Mbindyo JKN, Martin BR, Mallouk TE (2000) Chem Comm 2000:2445
133. Nikoobakht, Wang ZL, El-Sayed MA (2000) J Phys Chem B 104:8635
134. a) Wang XF, Zhang LD, Zhang J, Shi HZ, Peng XS, Zheng MJ, Fang J, Chen JL, Gao BJ (2001) J Phys D 34:418; b) Choi SH, Wang KL, Leung MS, Stupian GW, Presser N, Morgan BA, Robertson RE, Abraham M, King EE, Tueling MB, Chung SW, Heath JR, Cho SL, Ketterson JB (2000) J Vac Sci Technol A 18:1326
135. Masuda H, Yanagishita T, Yasui K, Nishio K, Yagi I, Rao TN, Fujishima A (2001) Adv Mater 13:247
136. a) Henry Y, Ounadjela K, Piraux L, Dubois S, George JM, Duvail JL (2001) Eur Phys J B 20:35; b) Cao HQ, Xu Z, Sang H, Sheng D, Tie CY (2001) Adv Mater 13:121; c) Yang SG, Zhu H, Ni G, Yu DL, Tang SL, Du YW (2000) J Phys D Appl Phys 33:2388; d) Puntes VF, Krishnan KM, Alivisatos AP (2001) Science 291:2115
137. Ounadjela K, Ferre R, Louail L, George JM, Maurice JL, Piraux L, Dubois S (1997) J Appl Phys 81:5455
138. a) Molares MET, Buschmann V, Dobrev D, Neumann R, Scholz R, Schuchert IU, Vetter J (2001) Adv Mater 13:62; b) Peng LQ, Ju X, Wang SC, Xian DC, Chen H, He YJ (1999) Chin Phys Lett 16:126; c) Setlur AA, Lauerhaas JM, Dai JY, Chang RPH (1996) Appl Phys Lett 69:345; d) Peng LQ, Ju X, Wang SC, Xian DC, Chen H, He YJ (1999) Chin Phys Lett16:126
139. Park SJ, Kim S, Lee S, Khim ZG, Char K, Hyeon TJ (2000) Am Chem Soc 122:8581
140. Zhang YF, Tang YH, Wang N, Lee CS, Bello I, Lee ST (2000) Phys Rev B 61:4518
141. Tang CC, Fan SS, Li P, de la Chapelle ML, Dang HY (2001) J Cryst Growth 224:1171
142. Gu Q, Dang HY, Cao J, Zhao JH, Fan SS (2000) Appl Phys Lett 76:3020; b) Wang N, Tang YH, Zhang YF, Lee CS, Bello I, Lee ST (1999) Chem Phys Lett 299:237; c) Wang N, Tang YH, Zhang YF, Lee CS, Lee ST (1998) Phys Rev B 58(N24):R16024
143. a) Krumeich F, Muhr HJ, Niederberger M, Bieri F, Nesper R (2000) Z Anorg Allg Chem 626:2208; b) Reinoso JM, Muhr HJ, Krumeich F, Bieri F, Nesper R (2000) Helv Chim Acta 83:1724; c) Niederberger M, Muhr HJ, Krumeich F, Bieri F, Gunther D, Nesper R (2000) Chem Mater 12:1995; d) Muhr HJ, Krumeich F, Schonholzer UP, Bieri F, Niederberger M, Gauckler LJ, Nesper R (2000) Adv Mater 12:231; e) Millet P, Henry JY, Mila F, Galy J (1999) J Solid State Chem 147:67678; f) Krumeich F, Muhr HJ, Niederberger M, Bieri F, Schnyder B, Nesper R (1999) J Am Chem Soc 121(N36):8324; g) Spahr ME, Stoschitzki-Bitterli P, Nesper R, Haas O, Novak P (1999) J Electrochem Soc 146:278,083; h) Spahr ME, Bitterli P, Nesper R, Muller M, Krumeich F, Nissen HU (1998) Angew Chem Int Ed 37:1263; i) Pillai KS, Krumeich F, Muhr HJ, Niederberger M, Nesper R (2001) Solid State Ionics 141:185
144. Lakshmi BB, Patrissi CJ, Martin CR (1997) Chem Mater 9:2544
145. Satishku BC, Govindaraj A, Nath M, Rao CNR (2000) J Mater Chem 10:2115–2119
146. a) Zhang M, Bando Y, Wada K (2001) J Mater Res 16:1408; b) Kasuga T, Hiramatsu M, Hoson A, Sekino T, Niihara K (1998) Langmuir 14:3160–3163; c) Hoyer P (1996) Langmuir 12:1411; d) Seo DS, Lee JK, Kim H (2001) J Cryst Growth 229:428; e) Li XH, Zhang XG, Li HL (2001) Chem J Chin Univ 22:130; f) Zhang M, Bando Y, Wada K (2001) J Mater Sci Lett 20:167; g) Zhang SL, Zhou JF, Zhang ZJ, Du ZL, Vorontsov AV, Jin ZS (2000) Chin Sci Bull 45:1533; h) Khitrov G (2000) MRS Bull 25:3; i) Imai H, Takei Y, Shimizu K, Matsuda M, Hirashima H (1999) J Mater Chem 9:2971; j) Lei Y, Zhang LD, Fan JC (2001) Chem Phys Lett 338:231; k) Lei Y, Zhang LD (2001) J Mater Res 16:1138; l) Lei Y, Zhang LD, Meng GW, Li GH, Zhang XY, Liang CH, Chen W, Wang SX (2001) Appl Phys Lett 78:1125; m) Hulteen JC, Martin CR (1997) J Mater Chem 7:1075; n) Kobayashi S, Hanabusa K, Hamasaki N, Kimura M, Shirai H, Shinkai S (2000) Chem Mater 12:1523
147. Lakshmi BB, Dorhout PK, Martin CR (1997) Chem Mater 9:857
148. Zheng MJ, Li GH, Zhang XY, Huang SY, Lei Y, Zhang LD (2001) Chem Mater 13:3859

149. a) Pu L, Bao XM, Zou JP, Feng D (2001) Angew Chem Int Ed 40:1490; b) Zheng MJ, Zhang LD, Zhang XY, Zhang J, Li GH (2001) Chem Phys Lett 334:298
150. Zheng MJ, Zhang LD, Zhang XY, Zhang J, Li GH (2001) Chem Phys Lett 334(N4/6):298
151. a) Li Y, Cheng GS, Zhang LD (2000) J Mater Res 15:2305; b) Huang MH, Wu YY, Feick H, Tran N, Weber E, Yang PD(2001) Adv Mater 13:113; c) Kong YC, Yu DP, Zhang B, Fang W, Feng SQ (2001) Appl Phys Lett 78:407–409; d) Li Y, Cheng GS, Zhang LD (2000) J Mater Res 15:2305; e) Li Y, Meng GW, Zhang LD, Phillipp F (2000) Appl Phys Lett 76:2011
152. Tang CC, Fan SS, de la Chapelle ML, Li P (2001) Chem Phys Lett 333:12
153. a) Zhang M, Bando Y, Wada K, Kurashima K (1999) J Mater Sci Lett 18:1911; b) Chang HJ, Chen YF, Lin HP, Mou CY (2001) Appl Phys Lett 78:3791; c) Wang LZ, Tomura S, Ohashi F, Maeda M, Suzuki M, Inukai K (2001) J Mater Chem 11:1465; d) Wu XC, Song WH, Wang KY, Hu T, Zhao B, Sun YP, Du JJ (2001) Chem Phys Lett 336:53; e) Liu ZQ, Xie SS, Sun LF, Tang DS, Zhou WY, Wang CY, Liu W, Li YB, Zou XP, Wang G (2001) J Mater Res 16:683–686; f) Wang ZL, Gao RPP, Gole JL, Stout JD (2000) Adv Mater 12:1938; g) Harada M, Adachi M (2000) Adv Mater 12:839; h) Lin HP, Mou CY, Liu SB (2000) Adv Mater 12:103; i) Zhang M, Bando Y, Wada K, Kurashima K (1999) J Mater Sci Lett 18:1911; j) Adachi M, Harada T, Harada M (1999) Langmuir 15:7097; k) Zhang M, Bando Y, Wada K (2000) J Mater Res 15:387
154. Park GS, Choi WB, Kim JM, Choi YC, Lee YH, Lim CB (2000) J Cryst Growth 220:494
155. Wang WH, Zhan YJ, Wang GH (2001) Chem Comm 2001:727
156. Vayssieres L, Beermann N, Lindquist SE, Hagfeldt A (2001) Chem Mater 13:233
157. Kwan S, Kim F, Akana J, Yang PD (2001) Chem Comm 2001:447
158. Zhang YF, Tang YH, Duan XF, Zhang Y, Lee CS, Wang N, Bello I, Lee ST (2000) Chem Phys Lett 323:180
159. a) Remskar M, Mrzel A, Skraba Z, Jesih A, Ceh M, Demsar J, Stadelmann P, Levy F, Mihailovic D (2001) Science 292:479; b) Hsu WK, Chang BH, Zhu YQ, Han WQ, Terrones H, Terrones M, Grobert N, Cheetham AK, Kroto HW, Walton DRM (2000) J Am Chem Soc122:10155; c) Seifert G, Terrones H, Terrones M, Jungnickel G, Frauenheim T (2000) Phys Rev Lett 85:146; d) Margulis L, Dluzewski P, Feldman Y, Tenne R (1996) J Microsc 181:68; e) Zhang Q, Huang RB, Liu ZY, Zheng LS (1995) Chem J Chin Univ16:1624; f) Feldman Y, Wasserman E, Srolovitz DJ, Tenne R (1995) Science 267:222; g) Mastai Y, Homyonfer M, Gedanken A, Hodes G (1999) Adv Mater 11:1010
160. Nath M, Govindaraj A, Rao CNR (2001) Adv Mater 13:283; b) Remskar M, Skraba Z, Stadelmann P, Levy F (2000) Adv Mater 12:814; c) Remskar M, Skraba Z, Sanjines R, Levy F (1999) Surf Rev Lett 6:1283; d) Feldman Y, Frey GL, Homyonfer M, Lyakhovitskaya V, Margulis L, Cohen H, Hodes G, Hutchison JL, Tenne R (1996) J Am Chem Soc 118:5362
161. Homyonfer M, Alperson B, Rosenberg Y, Sapir L, Cohen SR, Hodes G, Tenne R (1997) J Am Chem Soc 119:2693
162. a) Zhu YQ, Hsu WK, Terrones H, Grobert N, Chang BH, Terrones M, Wei BQ, Kroto HW, Walton DRM, Boothroyd CB, Kinloch I, Chen GZ, Windle AH, Fray DJ (2000) J Mater Chem 10:2570; b) Rothschild A, Sloan J, Tenne R (2000) J Am Chem Soc 122(N21):5169; c) Zhu YQ, Hsu WK, Grobert N, Chang BH, Terrones M, Terrones H, Kroto HW, Walton DRM, Wei BQ (2000) Chem Mater 12:1190; d) Mackie EB, Galvan DH, Adem E, Talapatra S, Yang GL, Migone AD (2000) Adv Mater 12:495; e) Seifert G, Terrones H, Terrones M, Jungnickel G, Frauenheim T (2000) Solid State Commun 114:245; f) Rothschild A, Frey GL, Homyonfer M, Tenne R, Rappaport M (1999) Synthesis of bulk WS2 nanotube phases. Mater Res Innovations 3:145
163. Tsirlina T, Feldman Y, Homyonfer M, Sloan J, Hutchison JL, Tenne R (1998) Fuller Sci Technol 6:157
164. Zhu YQ, Hsu WK, Terrones M, Firth S, Grobert N, Clark RJH, Kroto HW, Walton DRM (2001) Chem Commun 2001:121
165. a) Hsu WK, Zhu YQ, Firth S, Terrones M, Terrones H, Trasobares S, Clark RJH, Kroto HW, Walton DRM (2001) Carbon 39:1107; b) Hsu WK, Zhu YQ, Boothroyd CB, Kinloch I, Trasobares S, Terrones H, Grobert N, Terrones M, Escudero R, Chen GZ, Colliex C, Windle AH, Fray DJ, Kroto HW, Walton DRM (2000) Chem Mater 12:3541

166. Nath M, Rao CNR (2001) J Am Chem Soc 123:4841
167. Zhang WX, Yang ZH, Zhan JH, Yang L, Yu WC, Zhou GE, Qian YT (2001) Mater Lett 47:367
168. Li W, Kalia RK, Vashishta P (1996) Phys Rev Lett 77:2241
169. a) Sapp SA, Lakshmi BB, Martin CR (1999) Adv Mater 11:402; b) Prieto AL, Sander MS, Martín-González MS, Gronsky R, Sands T, Stacy AM (2001) J Am Chem Soc 123:7160
170. a) Davidson P, Gabriel JC, Levelut AM, Batail P (1993) Nematic liquid crystalline mineral polymers. Adv Mater 5:665; b) Davidson P, Gabriel JC, Levelut AM, Batail P (1993) Europhys Lett 21:317; c) Messer B, Song JH, Yang PD (2000) J Am Chem Soc 122:10,232
171. a) Wang SH, Yang SH (2000) Adv Mater Opt Electron 10:39; b) Wang SH, Yang SH (2000) Chem Phys Lett 322:567
172. Dloczik L, Engelhardt R, Ernst K, Fiechter S, Sieber I, Konenkamp R (2001) App Phys Lett 78:3687
173. Xu DS, Xu YJ, Chen DP, Guo GL, Gui LL, Tang YQ (2000) Chem Phys Lett 325; b) Li Y, Xu DS, Zhang QM, Chen DP, Huang FZ, Xu YJ, Guo GL, Gu ZN (1999) Chem Mater 11:3433
174. Shen CM, Zhang XG, Ki HL (2001) Mater Sci Eng A 303:19
175. a) Rubio A, Corkill JL, Cohen ML (1994) Phys Rev B 49:5081; b) Chopra NG, Luyken RJ, Cherrey K, Crespi VH, Cohen ML, Louie SG, Zettl A (1995) Science 269:966; c) Loiseau A, Willaime F, Demoncy N, Hug G, Pascard H (1996) Phys Rev Lett 76:4737; d) Suenaga K, Colliex C, Demoncy N, Loiseau A, Pascard H, Willaime F (1997) Science 278:653; e) Cumings J, Zettl A (2000) Chem Phys Lett 316:211
176. Shimizu Y, Moriyoshi Y, Komatsu S, Ikegami T, Ishigaki T, Sato T, Bando Y (1998) Thin Solid Films 316:178; b) Shimizu Y, Moriyoshi Y, Tanaka H, Komatsu S (1999) App Phys Lett 75:929
177. a) Han WQ, Bando Y, Kurashima K, Sato T (1998) Appl Phys Lett 73:3085; b) Han WQ, Bando Y, Kurashima K, Sato T (1999) Chem Phys Lett 299:368; c) Golberg D, Bando Y, Han W, Kurashima K, Sato T (1999) Chem Phys Lett 308:337; d) Han WQ, Redlich P, Ernst F, Ruhle M (1999) Chem Mater 11:3620; e) Golberg D, Bando Y, Bourgeois L, Kurashima K, Sato T (2000) Carbon 38:2017; f) Golberg D, Bando Y, Kurashima K, Sato T (2000) Chem Phys Lett 323:185
178. a) Chen Y, Gerald JF, Williams JS, Bulcock S (1999) Chem Phys Lett 299:260; b) Chen Y, Chadderton LT, FitzGerald J, Williams JS (1999) Appl Phys Lett 74:2960
179. Lourie OR, Jones CR, Bartlett BM, Gibbons PC, Ruoff RS, Buhro WE (2000) Chem Mater 12:1808
180. Terauchi M, Tanaka M, Suzuki K, Ogino A, Kimura K (2000) Chem Phys Lett 324:359
181. a) Li JY, Chen XL, Qiao ZY, Cao YG, He M, Xu T (2000) Appl Phys A 71:349; b) Chen CC, Yeh CC (2000) Adv Mater 12:738; c) Han WQ, Fan SS, Li QQ, Hu YD (1997) Science 277:1287; d) Chen et al. (2001) J Am Chem Soc123:2791; e) Li ZJ, Chen XL, Li HJ, Tu QY, Yang Z, Xu YP, Hu BQ (2001) Appl Phys A 72:629; f) He MQ, Minus I, Zhou PZ, Mohammed SN, Halpern JB, Jacobs R, Sarney WL, Salamanca-Riba L, Vispute RD (2000) Appl Phys Lett 77:3731; g) Chen XL, Li JY, Cao YG, Lan YC, Li H, He M, Wang CY, Zhang Z, Qiao ZY (2000) Adv Mater 12:1432; h) Tang CC, Fan SS, Dang HY, Li P, Liu YM (2000) Appl Phys Lett 77:1961; i) Peng HY, Zhou XT, Wang N, Zheng YF, Liao LS, Shi WS, Lee CS, Lee ST (2000) Chem Phys Lett 327:263; j) Cheng GS, Chen SH, Zhu XG, Mao YQ, Zhang LD (2000) Mater Sci Eng A 286:165; k) LilientalWeber Z, Chen Y, Ruvimov S, Washburn J (1997) Phys Rev Lett 79:2835; l) Li JY, Chen XL, Qiao ZY, Cao YG, Lan YC (2000) J Cryst Growth 213:408; m) Cheng GS, Zhang LD, Chen SH, Li Y, Li L, Zhu XG, Zhu Y, Fei GT, Mao YQ (2000) J Mater Res 15:347; n) Duan XF, Lieber CM (2000) J Am Chem Soc 122:188; o) Lee SM, Lee YH, Hwang YG, Elsner J, Porezag D, Frauenheim T (1999) Phys Rev B 60:7788; p) Zhu J, Fan S (1999) J Mater Res 14:1175; q) Lee SM, Lee YH, Hwang YG, Lee CJ (1999) J Korean Phys Soc 34:S253; r) Bedarev DA, Kogitskii SO, Lundin VV (1999) Tech Phys Lett 25:385
182. a) Han WQ, Fan SS, Li QQ, Gu BL, Zhang XB, Yu DP (1997) Appl Phys Lett 71:2271; b) Wu XC, Song WH, Zhao B, Huang WD, Pu MH, Sun YP, Du JJ (2000) Solid State Commun 115:683
183. Duan XF, Huang Y, Cui Y, Wang JF, Lieber CM (2001) Nature 409:66

184. Duan X, Lieber CM (2000) Adv Mater 12:298
185. Shi WS, Zheng YF, Wang N, Lee CS, Lee ST (2001) Appl Phys Lett 78:3304–3306
186. a) Pham-Huu C, Keller N, Ehret G, Ledoux MJ (2001) J Catal 200:400; b) Li YB, Xie SS, Wei BQ, Lian GD, Zhou WY, Tang DS, Zou XP, Liu ZQ, Wang G (2001) Solid State Commun 119:51; c) Gao YH, Bando Y, Kurashima K, Sato T (2001) Scr Mater 44:1941; d) Zhang YJ, Wang NL, He RR, Chen XH, Zhu (2001) J Solid State Commun 118:595; e) Wu XC, Song WH, Huang WD, Pu MH, Zhao B, Sun YP, Du JJ (2001) Mater Res Bull 36:847; f) Li YB, Xie SS, Zou XP, Tang DS, Liu ZQ, Zhou WY, Wang G (2001) J Cryst Growth 223:125; g) Shi WS, Zheng YF, Peng HY, Wang N, Lee CS, Lee ST (2000) J Am Ceram Soc 83:3228; h) Wang ZL, Dai ZR, Gao RP, Bai ZG, Gole JL (2000) Appl Phys Lett 77:3349; i) Liang CH, Meng GW, Zhang LD, Wu YC, Cui Z (2000) Chem Phys Lett 329:323; j) Pan ZW, Lai HL, Au FCK, Duan XF, Zhou WY, Shi WS, Wang N, Lee CS, Wong NB, Lee ST, Xie SS (2000) Adv Mater 12:1186; k) Hu JQ, Lu QK, Tang KB, Deng B, Jiang RR, Qian YT, Yu WC, Zhou GE, Liu XM, Wu JX (2000) J Phys Chem B 104:5251; l) Zhou XT, Wang N, Au FCK, Lai HL, Peng HY, Bello I, Lee CS, Lee ST (2000) Mater Sci Eng A 286:119; m) Tang CC, Fan SS, Dang HY, Zhao JH, Zhang C, Li P, Gu Q (2000) J Cryst Growth 210:595; n) Zhou XT, Lai HL, Peng HY, Au FCK, Liao LS, Wang N, Bello I, Lee CS, Lee ST (2000) Chem Phys Lett 318:58; o) Lai HL, Wong NB, Zhou XT, Peng HY, Au FCK, Wang N, Bello I, Lee CS, Lee ST, Duan XF (2000) Appl Phys Lett 76:294; p) Lu QY, Hu JQ, Tang KB, Qian YT, Zhou G, Liu XM, Zhu JS (1999) Appl Phys Lett 75:507; q) Zhou XT, Wang N, Lai HL, Peng HY, Bello I, Wong NB, Lee CS, Lee ST (1999) Appl Phys Lett 74:3942; r) Meng GW, Zhang LD, Mo CM, Zhang SY, Qin Y, Feng SP, Li HJ (1998) J Mater Res 13:2533; s) Han WQ, Fan SS, Li QQ, Liang WJ, Gu BL, Yu DP (1997) Chem Phys Lett 265:374
187. a) Liang CH, Meng GW, Chen W, Wang YW, Zhang LD (2000) J Cryst Growth 220:296; b) Qi SR, Huang XT, Gan ZW, Ding XX, Cheng Y (2000) J Cryst Growth 219:485; c) Gao Y, Liu J, Shi M, Elder SH, Virden JW (1999) Appl Phys Lett 74:3642
188. a) Fukunaga A, Chu S, McHenry MEJ (1999) Mater Sci Lett 18:431; b) Nesting DC, Kouvetakis J, Smith DJ (1999) Appl Phys Lett 74:958; c) Fukunaga A, Chu SY, McHenry ME (1998) J Mater Res 13:2465; d) Wong EW, Nor BW, Burns LD, Lieber CM (1996) Chem Mater 8:2041; e) Ata M, Hudson AJ, Yamaura K, Kurihara K (1995) Jap J Appl Phys 34:4207; f) Liu MG, Cowley JM (1995) Carbon 33:749; g) Dai HJ, Wong EW, Lu YZ, Fan SS, Lieber CM (1995) Nature 375:769; h) Liu MQ, Cowley JM (1995) Carbon 33:225; i) Ata M, Kijima Y, Hudson AJ, Imoto H, Matsuzawa N, Takahashi N (1994) Adv Mater 6:590; j) Seraphin S, Zhou D, Jiao J, Withers JC, Loutfy R (1993) Nature 362:503